A Thesis

On

WEAR CHARACTERISTIC OF DUAL REINFORCED PARTICLES (DRP) ALUMINUM ALLOY

Submitted in the partial fulfillment of requirement for the degree of

Master of Technology

in

Material Science and Metallurgical Engineering

by

Vipin Sharma

(600902014)

Under the supervision of

Dr. O. P. Pandey

(Prof. & Head)

School of Physics and Materials science

Thapar University, Patiala, (Punjab), INDIA

July-2011

Certificate

This is to certify that this thesis entitled "**Wear characteristic of Dual Reinforced Particles (DRP) aluminum alloy**" which is being submitted by **Mr. Vipin Sharma** in fulfillment of the requirement for the award of degree of Master of Technology in school of physics and material science, Thapar university, Patiala, (Punjab) is an exclusive record of candidate's own research under our supervision. The thesis in part or in full has not been submitted in any other university or in institute for the award of any degree. The thesis is fit to be considered for the award of degree of Master of Technology.

This is to certify that the above statement made by the candidate is correct and true to best of my knowledge.

Dr. O. P. Pandey
(Supervisor)

Countersigned By:

Dr. O.P. Pandey
Prof. & Head
School of Physics & Material Science
Thapar University
Patiala, Punjab

Dr. S. K. Mohapatra
Dean Academic Affairs
Thapar University
Patiala,Punjab

ACKNOWLEDGEMENT

With deep regards and profound respect, I avail this opportunity to express my deep sense of gratitude and indebtedness to **Dr. O.P Pandey, Professor and Head, School of Physics and Material Science**, for his keen interest, strong motivation and constant encouragement during the course of the work. He always bestowed parental care upon us and evinced keen interest in solving our problems. An erudite teacher, a magnificent person and a strict disciplinarian, we consider ourselves fortunate to have worked under his supervision.

I thank him for his great patience, constructive criticism and useful suggestions apart from invaluable guidance to me.

I would also like to thank **Dr. Kulvir Singh, Associate Professor, School of Physics and Materials Science** for his constant guidance and encouragement. I am also thankful to **Dr. Manoj Sharma, Dr. Puneet Sharma, Dr. B. N. Chudasama, Dr. Sunil Kumar** and all the faculty members of School of Physics and Materials Sciences for their constructive suggestions at different stages of this work.

It gives me immense pleasure to express my special thanks to **Lab Supdt. Mr. P. K. Singh, Mr. Ranvir Singh Panwar** (Ph.D.scholar), **Ms. Meenu** and **Mr. Suresh Kumar** who always took keen interest in guiding me during my work.

I am extremely thankful to research scholar **Mr. Ravi Shukla, Mrs. Gurbinder Kaur, Mr. Akshay Kumar, Mr. Harjinder, Ms. Mani Mahajan, Mr. Gaurav Singla, Ms. Samita Thakur, Ms. Chandani and Mr. Paramjyot Kumar Jha** of Thapar University for constant support. Last but not the least, I also thank to staff of SPMS **Mrs. Praveen Kumari, Mr. Jant singh, Mr. Indermani and Mr. Vishal**

I would like to convey my sincere gratitude to my friends and colleagues **Mr. Mintu Tyagi, Mr. Vijay Kumar Baliyan, Mr. Akshay Kumar, Mr. Arvind Kumar and Ms. Richa Sharma** for their support and their timely help and valuable discussions.

And above all, I pay my regards to the **Almighty** for his love and blessings.

(Vipin Sharma)

ABSTRACT

The present investigation aims to find the combined effect of dual reinforced particle in aluminium alloy LM13 on the wear behavior. The composites are fabricated by varying the percentage of reinforcement of silicon carbide and zircon sand particles. The wear behavior of composites is compared with each other to find out optimum combination of dual reinforced particles. Particles of 20-32 μm size are used in the present study. The wear test was carried out on pin-on disk machine. Wear track and debris are analyzed by SEM to study the wear mechanism. Study reveals that a combination of 3.75% zircon sand and 11.25% silicon carbide reinforced composite exhibits better wear resistance while 7.5% zircon sand and 7.5% silicon carbide reinforcement decreases the wear resistance. It is also observed that zircon sand and silicon carbide particles provide effective nucleation site for the eutectic silicon. Microstructural examination shows globular and finely distributed eutectic silicon in the vicinity of the reinforced particles.

CONTENTS

LIST OF FIGURES

LIST OF TABLES

CHAPTER-1

INTRODUCTION

1. Introduction

Composites are the class of materials that evolved with the existence of nature. Nature inspires the today's composite advancement in the field of aeronautical, aerospace, automotive and structural sector. Composites are engineered materials that have been designed to provide significantly higher specific stiffness and specific strength i.e. higher structural efficiency relative to previously available structural materials. As a common practical definition, composite materials may be restricted to emphasize those materials that contain a continuous matrix constituent that binds together and provides form to an array of a stronger, stiffer reinforcement constituent. The resulting composite material has a balance of structural properties that is superior to either constituent material alone [1]. Reinforced concrete is an excellent example of a composite structure in which the concrete and steel still retain their identities.

Composites are broadly classified on the basis of matrix and reinforcement used. When Metal is used as a matrix, composites are classified as metal matrix composite.

1.1 Metal matrix composites

A metal matrix composite (MMC) is material with at least two constituent parts, one being a metal. The other material may be a different metal or another material, such as a ceramic or organic compound. Metals mainly used for matrix are Aluminium, Magnesium, Steel, Titanium etc. and reinforcement used are long fiber, whisker or discontinuous particle. Generally ceramic reinforcement are used in metal matrix composites like silicon carbide, boron, alumina, silicon nitride, boron carbide, boron nitride, silica sand, zircon sand etc. Metal-matrix composites (MMCs) exhibit the ability to withstand high tensile and compressive stresses by the transfer and distribution of the applied load from the ductile matrix to the reinforcement phase [2]. MMCs combine metallic properties of matrix alloys like ductility and toughness with ceramic properties of reinforcement's mainly high strength and high modulus which leads to greater strength in shear and compression and higher service-temperature capabilities. Thus, they have significant scientific, technological and commercial importance [1-2]

Seashell are naturally existing composite from the very beginning of human evolution, they are attracting and inspiring engineers even today by possessing better mechanical properties. Bone is also a natural composite, which shows the nature intelligence in using composite as a structural frame for body.

1.1.1 Matrix

The matrix is the monolithic material into which the reinforcement is embedded and is completely continuous. This means that there is a path through the matrix to any point in the material, unlike two materials sandwiched together. In structural applications, the matrix is usually a lighter metal such as aluminum, magnesium, or titanium, and provides a compliant support for the reinforcement. In high temperature applications, cobalt and cobalt-nickel alloy matrix are common.

1.1.2 Reinforcement

The reinforcement material is embedded into the matrix. The reinforcement does not always serve a purely structural task (reinforcing the compound), but is also used to change physical properties such as wear resistance, friction coefficient, or thermal conductivity. The reinforcement can be either continuous, or discontinuous. Discontinuous MMCs can be isotropic, and can be worked with standard metalworking techniques, such as extrusion, forging or rolling. In addition, they may be machined using conventional techniques, but commonly would need the use of polycrystaline diamond tooling. Continuous reinforcement uses monofilament wires or fibers such as carbon fiber or silicon carbide. Because the fibers are embedded into the matrix in a certain direction, the result is an anisotropic structure in which the alignment of the material affects its strength. One of the first MMCs used boron filament as reinforcement. Discontinuous reinforcement uses "whiskers", short fibers or particles. The most common reinforcing materials in this category are alumina and silicon carbide [3].

1.2 Processing Routes

MMC manufacturing can be broken into three types: solid, liquid and vapor.

Solid state methods

- Powder metallurgy: Powdered metal and discontinuous reinforcement are mixed and then bonded through a process of compaction, degassing and thermo-mechanical treatment
- Foil diffusion bonding: Layers of metal foil are sandwiched with long fibers, and then pressed through to form a matrix.

Liquid state methods

- Electroplating / Electroforming: A solution containing metal ions loaded with reinforcing particles is co-deposited forming a composite material.
- Stir casting: Discontinuous reinforcement is stirred into molten metal, which is allowed to solidify.
- Squeeze casting: Molten metal is injected into a form with fibers preplaced inside it.

- Spray deposition: Molten metal is sprayed onto a continuous fiber substrate.
- Reactive processing: A chemical reaction occurs, with one of the reactants forming the matrix and the other the reinforcement.

Vapor deposition

- Physical vapor deposition: The fiber is passed through a thick cloud of vaporized metal, coating it [1-3].

1.3 Advantages of MMCs

Compared to monolithic metals, MMCs have:

- Higher strength-to-density ratios
- Higher stiffness-to-density ratios
- Better fatigue resistance
- Better elevated temperature properties
- Lower creep rate

The advantages of MMCs over polymer matrix composites are:

- Higher temperature capability
- Fire resistance
- Higher transverse stiffness and strength
- No moisture absorption
- Higher electrical and thermal conductivities
- Better radiation resistance.

1.4 Disadvantages of MMCs

Some of the disadvantages of MMCs compared to monolithic metals and polymer matrix composites are:

- Higher cost of some material systems
- Relatively immature technology
- Complex fabrication methods for fiber-reinforced systems (except for casting)
- Limited service experience [4]

1.5 Application of MMCs

- Carbide drills are often made from a tough cobalt matrix with hard tungsten carbide particles inside.

- Some tank armors may be made from metal matrix composites, probably steel reinforced with boron nitride. Boron nitride is a good reinforcement for steel because it is very stiff and it does not dissolve in molten steel.

- Some automotive disc brakes use MMCs.

- The F-16 Fighting Falcon uses monofilament silicon carbide fibres in a titanium matrix for a structural component of the jet's landing gear.

- Specialized Bicycles have used aluminium MMC compounds for their top of the range bicycle frames for several years.

In comparison with conventional polymer matrix composites, MMCs are resistant to fire can operate in wider range of temperatures, do not absorb moisture, have better electrical and thermal conductivity, are resistant to radiation, and do not display outgassing. On the other hand, MMCs tend to be more expensive, the fiber-reinforced materials may be difficult to fabricate, and the available experience in use is limited [1-4].

2. Aluminium matrix composites (AMC's)

Aluminum is an important industrial material that has the advantage of being relatively light compared to other metals, and is used in a wide variety of areas, for example architecture, transportation, and packaging. However, aluminum suffers from low strength, stiffness, and wear, and thus it fails in applications where these properties are needed. Strengthening of aluminum by the addition of small quantities of soluble metals or alloying elements is not enough to compete with other strong alloys such as steel [3].

Aluminum matrix composites permit the achievement of new properties and controlled characteristics by the addition of special materials (reinforcement) that are not soluble and do not react with aluminum and its alloys [1-4]. In these composites, each phase (Al-matrix and reinforcement) maintains its own characteristics, whereas the composite characteristics are unique, representing a combination of both constituents. According to the composite theory, the physical and mechanical properties of AMCCs can be tailored by changing the reinforcement type, shape, and volume of fraction. Unless processing difficulties result, unlimited variation in properties can be obtained. Most of the work available on metal matrix composite is focused on composites with aluminum matrix, because they can achieve the main objective of high specific strength [3].

The aluminum metal-matrix composites are broadly classified as:

(a) Continuous fibers
(b) Whiskers/discontinuous fibers
(c) Particulates.

2.1 Continuous fibre-reinforced AMCs

In this type of composite the reinforcements are in the form of continuous fibres (of alumina, SiC or carbon) with a diameter less than 20 µm. The fibres can either be parallel or pre woven, braided prior to the production of the composite. AMCs having fibre volume fraction up to 40% are produced by squeeze infiltration technique. The continuous fiber reinforced Al MMCs offer the best combination of strength and stiffness. However, the cost of these systems is very high, mainly because of the high costs of the continuous fibers and of the production. These materials are mainly of interest for aerospace or military industries, where weight savings and very specific properties are of great importance than material cost. Among the attractive properties of these materials the most important one is the elevated

temperature strength. The possibility of mechanical working on these materials is small, and they are hardly recyclable [5].

2.2 Whiskers/discontinuous fibers AMCs

These contain reinforcements with an aspect ratio of greater than 5, but are not continuous. Short alumina fibre reinforced aluminium matrix composites is one of the first and most popular AMCs to be developed and used in pistons. The whisker based composites are more costly than the particulate based ones, but offer higher strength in general. Compared to discontinuous reinforcements, such as polycrystalline flakes, particulates or chopped fibers, single crystal whiskers usually have a much greater tensile strength and are generally used to produce the highest strength discontinuously reinforced MMCs. It is easier to recycle these materials compared to the continuous fiber reinforced material when the correct matrix and reinforcement combination is selected [3-5].

2.3 Particulates reinforced AMCs.

These composites generally contain equiaxed ceramic reinforcements with an aspect ratio less than about 5. Ceramic reinforcements are generally oxides or carbides or borides (Al_2O_3 or SiC or TiB_2) and present in volume fraction less than 30% when used for structural and wear resistance applications. However, in electronic packaging applications reinforcement volume fraction could be as high as 70%. In general, PAMCs are manufactured either by solid state (P/M processing) or liquid state (stir casting, infiltration and in-situ) processes.

PAMCs are less expensive compared to CFAMCs. Mechanical properties of PAMCs are inferior compared to whisker/short fibre/con AMCs but far superior compared to unreinforced aluminium alloys. These composites are isotropic in nature and can be subjected to a variety of secondary forming operations including extrusion, rolling and forging. Particulate–reinforced Al MMCs are of particular interest due to their ease of fabrication, lower costs, and isotropic properties. However, the improvement in strength does not seem to be high and the strain to failure and fracture are low compared to the matrix material. The particulate reinforced Al MMCs are easier to recycle than the fiber reinforced ones provided that an appropriate matrix and particulate reinforcement combination is selected.
Overall strength of such particle- reinforced MMCs depends on size of the particles, the interparticle spacing, volume fraction of the particles, and the nature of matrix and reinforcement interface. Matrix properties including the work hardening coefficient, which improves the effectiveness of the reinforcement constraint, are also important [4-5]

2.4 Processing route for AMCs

Processing route for AMCs are similar to MMCs, So only stir casting process is described as it used in this study. Mainly the following are used

- Powder Metallurgy
- Stir Casting
- Spray Co-deposition

2.5 Stir Casting

Stir casting is the one of the extensively used and economical synthesis technique for fabricating the particulate reinforced aluminium reinforced composite. It is simpler as compared to other available techniques and flexibility in tailoring the desired properties in the composite.

In stir casting the aluminium is placed in a graphite crucible and melted in a resistance furnace. When the melt is in liquid state, the impeller is introduced in to the melt. The impeller is rotated at specified rotation to create a vortex in the melt. The reinforcement particles are introduced in to the melt through the side of the vortex formed. The vortex sucks the particle and distributes it in to the melt. The vortex method is one of the better known approaches used to create and maintain a good distribution of the reinforcement material in the matrix alloy. Stirring for sometime followed by mixing is done to obtain homogeneous distribution of particles. The next step is the solidification of the melt containing suspended particles under selected conditions to obtain the desired distribution of the dispersed phase in the cast matrix [6].

In preparing metal matrix composites by the stir casting method, there are several factors that need considerable attention, including

- Porosity
- The difficulty of achieving a uniform distribution of the reinforcement material
- Wettability between the two main substances

In order to achieve the optimum properties of the metal matrix composite, the distribution of the reinforcement material in the matrix alloy must be uniform, and the wettability or bonding between these substances should be optimised. The porosity levels need to be minimised, and chemical reactions between the reinforcement materials and the matrix alloy must be avoided [6-7].

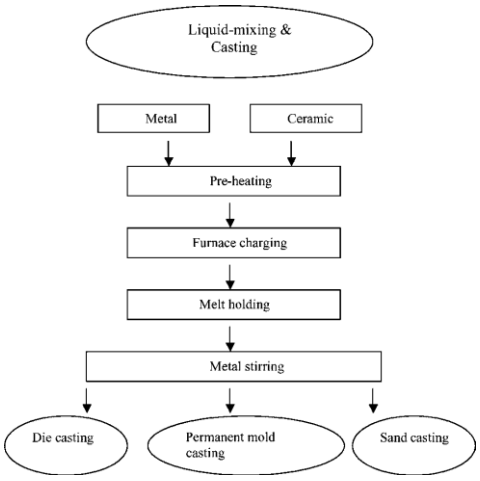

Fig.1: The process of stir casting [7]

2.5.1 Porosity

Porosity is a common feature of Stir cast metal matrix composites and strongly influences their properties and applications. The volume fraction of porosity, and its size and distribution in a cast metal matrix composite play an important role in controlling the material's mechanical properties. This kind of a composite defect can be detrimental also to the corrosion resistance of the casting. The presence of pores is accompanied by a decrease in mechanical properties, i.e., a drop in strength and ductility of the materials [8].

Porosity levels must, therefore, be kept to a minimum. Porosity cannot be fully avoided during the casting process, but it can, however, be controlled. In general, porosity arises from three causes:

(a) Gas entrapment during mixing,

(b) Hydrogen evolution, and

(c) Shrinkage during solidification.

Other factors are like

- Particle clustering, which hinder the liquid metal flow during solidification
- Poor wettability between reinforced particle and matrix
- High stirring speed, this may entraps the air in the liquid melt

Not only the total volume percentage of porosity influences the degradation of properties but also size, shape and interconnectivity of the porosity play an important role. The influence of porosity on the wear behavior of materials also depends on wear conditions. Pores act as lubricant reservoirs in wet sliding conditions, which provide considerable advantage in wear processes. In contrast, in dry sliding condition, the wear rate increases gradually with increase in volume fraction of porosity content due to its combined effect on both the real area of contact and subsurface cracking. With an increase in porosity, the load bearing cross-section decreases. The wear coefficient increases with the increase in contact pressure between the

frictional pairs due to the decrease in load bearing cross-section. Also, the emergence of stress concentrations around pores leads to accelerated wear and the level is determined by the pore size, shape and orientation [8-9].

Under certain conditions, porosity may act as a trap for wear debris. Trapping of wear debris in surface pores decreases wear rate by decreasing the contact pressure and plastic deformation near pores. The size and distribution of porosity in the matrix also play an important role in wear. It is found that isolated porosity is apparently beneficial for wear resistance compared to the interconnected one [6-9].

(a) (b)

Fig. 2: The entrapment of air during stirring (a) before stirring (b) during stirring

2.5.2 Particle distribution

Homogeneous particle distribution can be achieved by optimizing several parameters such as blade angle, number of blades, position of the stirrer, stirring speed and time, size of the particle and methods to enhance wettability. Mostly focus is on stirring, in general stirring helps in two ways: to transfer particles into the liquid metal, and to maintain the particles in suspension. Several types of stirrers are available for stirring purposes. In some cases, the stirrers are design in order to provide a high degree of axial flow. A vortex created during stirring can suck in even non-wetting particles and also bubbles in to a molten alloy. Particles often attached to the bubbles, counteracting the buoyancy which would normally help them to float out of the melt. As a result, it has been observed that porosity content in a stircast composite varies almost linearly with particle content. It is necessary to create turbulence during stirring, but it should be only in the bottom region of the fluid [8].

2.5.3 Wettability

Wettability can be defined as the ability of a liquid to spread on a solid surface and represent the exent of intimate contact between a liquid and a solid. Good wetting between the solid ceramic phase and the liquid metal matrix is an essential condition for the generation of a satisfactory bond between these two during casting. Wettability is decreased by metal oxide layer and gas envelope on the particle.

Several approaches have been taken to promote wetting of reinforcement particles with a molten matrix alloy. These include:

- The addition of alloying elements to the matrix alloy
- Coating of the ceramic particles
- Treatment of the ceramic particles (preheating)

To promote wettability selection of suitable alloy and particle preheating are applied in normal course of practice [10].

2.6 Two Step Stir casting

The furnace temperature was first raised above the liquidus to melt the alloy scraps completely and was then cooled down just below the liquidus to keep the slurry in a semi-solid state. At this stage the preheated particles were added and mixed manually by a rod. Manual mixing was used because it was very difficult to mix using automatic device when the alloy was in a semi-solid state.
After sufficient manual mixing was done, the composite slurry was reheated to a fully liquid state and then automatic mechanical mixing was carried out for about 10 minutes at a normal stirring rate of 600 rpm. The stirring was continued before the composite is poured in to a metal mould.

Two step stir casting have an advantage in terms of promoting wettability, reduction of porosity and homogeneous distribution of particles [11-13].

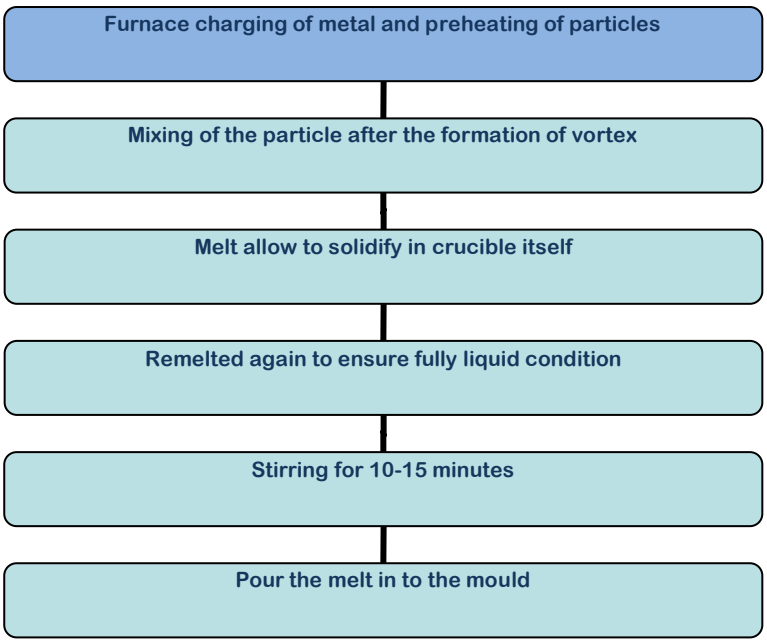

Fig.3: Two step stir casting process

CHAPTER-3

LITERATURE REVIEW

Rao et. al [1] evaluated the effect of sliding distance on the wear and friction behavior of as cast and heat-treated Al–SiCp composites using pin-on-disc wear testing machine, giving emphasis on the parameters such as wear rate and coefficient of friction as a function of sliding distance (0–5000 m) at different applied pressures of 0.2, 0.6, 1.0 and 1.4 MPa and at a fixed sliding speed of 3.35 m/s. The results revealed that the heat-treated composite exhibited superior wear properties than the base alloy, while the coefficient of friction followed an opposite trend. Moreover, the wear rate of the composite is noted to be invariant to the sliding distance and increased with applied pressures.

Celis et. al [2] Studied the tribological behavior of sintered aluminum metal matrix composites (MMCs) containing various volume fractions of particles made of complex metallic alloys (CMAs) was investigated in a reciprocating dry sliding tribo-tester operated in ambient air against 10mmdiameter Al_2O_3 balls. The Al-based MMCs tested contained either 15μm size AlCuFeB or 25μm size AlCuFeCr-particles. An improvement in the dry sliding wear resistance of aluminum was achieved by the incorporation of these CMA-particles acting as a second phase reinforcement. The wear resistance depends on the volume fraction of CMA-particles but not on their composition, nano-hardness or size. These Al-based MMCs containing CMA-particles exhibit however a higher coefficient of friction than pure aluminum under dry sliding against a ceramic counterbody.

Emamy et al. [3] fabricated the nanocomposites of AA 2024 aluminum alloy matrix reinforced with different volume fractions of nanometric $MoSi_2$ intermetallic particles ranging from 0 to 5% by using mechanical alloying technique. For comparison, samples without reinforcing particles and mechanical alloying and a sample with micrometric $MoSi_2$ particles were also synthesized. The prepared composite powders were consolidated by cold and hot pressing and then heat treated to solution and aged condition (T6).

The results indicated that although T6 heat treatment increases the hardness of all samples compared to as hotpressed (HP) condition, the age-hardenability (aging induced hardness improvement) decreases after mechanical alloying and with increasing $MoSi_2$ volume fraction due to the high dislocation density produced during mechanical alloying. With increasing the volume fraction of nano-sized $MoSi_2$ particles up to 3–4%, the hardness of the composites continuously increases and then declines most probably due to the particle agglomeration. The wear sliding test disclosed that the wear resistance of all specimens in T6 condition is higher than that of hotpressed condition and increases with increasing $MoSi_2$ content.

Suresha et al. [4] studied the effect of % reinforcement, load, sliding speed and sliding distance on stir cast Al–SiC–Gr hybrid composites, Al–Gr and Al–SiC composites. Parametric studies indicate that the wear of hybrid composites has a tendency to increase beyond% reinforcement of 7.5% as its values are 0.0242 g, 0.0228 g and 0.0234 g respectively at 3%, 7.5% and 10% reinforcement. The corresponding values are 0.0254 g, 0.0240 g and 0.0242 g in Al–Gr composites and 0.0307 g, 0.0254 g and 0.0221 g in Al–SiC composites, clearly indicating that hybrid composites exhibit better wear characteristics. Increase of speed reduces wear and increase of either load or sliding distance or both increases wear.

Vencl et al. [5] examined and compare the structural, mechanical and tribological properties of heat treated particulate composites of A356 aluminium alloy as a matrix reinforced with ceramic particles (Al_2O_3, SiC) and graphite particles. Composites are prepared by compocasting process

The study shows that heat treatment affected microstructure of the composites matrix. The fracture of the composites matrix was ductile, while transition from ductile to brittle fracture occurred in the zone of reinforcing particles. The values of elasticity modulus of all the composites were higher in relation to the matrix alloy. It was also established that wear resistance and coefficient of friction were better at the SiC particulate composites than at the Al_2O_3 particulate composite, while the addition of graphite particles improved tribological properties further.

Rams et al. [6] studied the dry sliding wear of an AA 6061 alloy reinforced with both modified SiC particles and metal coated carbon fibres. SiC particles were coated with a silica layer deposited through a sol–gel procedure to increase the processability of the composite and to enhance the particle–matrix interfacial resistance. The metallic coatings on carbon fibres were made of copper or nickel phosphorus which was deposited through an electroless process. The metallic coatings favoured the wetting of the fibres during processing and then dissolved in the aluminium matrix forming intermetallic compounds that increased its hardness. Wear behaviour of AA 6061–20%SiC and AA 6061–20%SiC–2%C was compared with that of the composites with the same reinforcement content but using coated particles and fibres. The influence that the modification of the matrix because of the incorporation of coatings on the reinforcements had on the mild wear behaviour was investigated. The wear resistance of the composites increased when carbon fibres were added as secondary reinforcement and when coated reinforcements were used.

Pang et al. [7] used simulations to investigate the mechanical properties of aluminum matrix nanocomposites reinforced with nanosized silicon carbide. Study shows that reducing the size of the particles to the nanoscale dramatically increases the mechanical strength of these

composites even at low particle volume fractions. The mechanical response of aluminum matrix reinforced with nanosized silicon carbide is analyzed using plane strain; discrete dislocation plasticity. The numerical results show improvements in the mechanical strength of the nanocomposite material with increasing particle volume fraction and decreasing particle size.

Dwivedi et al. [8] statistically analyzed the material related parameter on dry reciprocating wear behavior of aluminium silicon alloy matrix with SiC reinforced particles. The analysis shows that the applied load, sliding distance, reciprocating velocity and percentage silicon weight in composite are the four important and controlling factors; counter surface temperature has a minor effect on the wear of the composite specimens in dry condition. The two-factor interactions have strong effect on the wear of the composite especially the interactions between load and sliding distance (8.07%) and that between load and weight percent silicon (3.28%) are influencing more compared to the other interactions.

Rajan et al. [9] studied the hardness of stir and centrifugally cast Al-SiCp functionally graded metal matrix composites with graded distribution of SiC particles near the outer periphery of the casting. Study shows that maximum of 45 and 40% SiC particles are obtained near the outer periphery of the Al(356)-SiC and Al(2124)-SiC FGMMC casting respectively. The maximum hardness obtained at the outer periphery after heat treatment for Al(356)-SiC and Al(2124)-SiC FGMMC are 155 BHN and 145 BHN respectively. The freezing range of the matrix alloy has been found to dictate the nature of transition from particle enriched to depleted zone.

Farhat et al. [10] developed a model to explain the relationship between porosity and pore size. Al-Si alloy with different porosity levels was prepared using powder metallurgy technique. Dry sliding wear behavior was investigated against AISI 52100 bearing steel ball. It was found that the wear rate gradually rises with surface porosity and then drops as porosity and pore size reach critical levels. When pore size is in the same order of magnitude as the contact area between the counter-face and the specimen, the counter-face slides in to the pores; hence, pores become less effective in generating wear debris.

Hirotaka Kato [11] investigated the effects of supplying iron-oxide or iron particles and influence of the size of supplied powders on the transition from severe running-in to mild steady wear. The test is carried on pin-on disk machine. It was found that the supply of fine oxide particles with diameters of 0.5 μm and less accelerated the severe–mild wear transitions. The sliding distance of the severe–mild wear transition was reduced when finer particles were supplied, suggesting that fine particles easily form compacted layers on the wear surface. On the other hand, employing oxide particles of 1μm, no severe–mild wear transition was observed, producing a wear curve similar to that observed in the test, where no particles were supplied.

Das et al. [12] reported a comparative study on abrasive wear behavior of aluminum metal matrix composite reinforced with alumina and zircon sand particles. Study mainly focused on the effect of particle size of the reinforcement on the wear and hardness of the composite. Study shows that Abrasive wear resistance of both the composites improves with the decrease in particle size. It is observed that the alumina particle reinforced composite shows relatively poor wear resistance property compared to zircon-reinforced composite. Decrease in particle size improves wear resistance property for both alumina and zircon reinforced composites as smaller particle reinforced composite has higher hardness and is more efficient in blunting SiC abrading surface. Zircon reinforced composite shows better wear resistance than alumina reinforced composite due to its superior particle–matrix bonding.

Sharma et al. [13] studied the unlubricated sliding wear behaviour of zinc–aluminium. Alloy composites reinforced with zircon particles of size 30–50 μm. The content of zircon in the alloy was varied from 1–5% in steps of 2wt. %. The liquid metallurgy technique was used to fabricate the composites. The results indicated that the wear rate of the composites was lesser than that of the matrix alloy and it further decreased with the increase in zircon content. However, the material loss in terms of wear rate and the wear volume increased with the increase in load and sliding distance, respectively, both in the case of composites and the alloy. Increase in the applied load increased the wear severity by changing the wear mechanism from abrasion to particle cracking induced delamination wear. It was found that with the increase in zircon content, the wear resistance increased monotonically.

Sharma and Das [14] studied the age hardening behavior of Al-4.5%Cu alloy composite reinforced with zircon sand particulates and produced by stir casting route. Composite has been investigated in different quenching media viz, water, oil, and salt brine solution (7 wt %). The results of ageing demonstrate that the microhardness of age hardenable Al-Cu based alloy composites depend on the quenching medium in which they are heat treated. Under all the heat treatment conditions, the microhardness increased with the ageing time to a peak value and then decreased with a prolonged ageing time. Salt brine quenching is faster as compared to water and oil, even if higher strength is obtained but cannot be used for complex shapes and thin sections where oil quenching is the alternative due to minimum distortion and cracking problems. Thermal cycling studies of the composite at 25–540 °C have been also carried out to determine the extent of quenching of the matrix after each solution heat treatment cycle while varying the quenching media.

Mondal and Das [15] studied high stress abrasive wear behaviour of aluminium alloy (ADC-12)–SiC particle reinforced composites as a function of applied load, reinforcement size and volume fraction, and has been compared with that of the matrix alloy. Two different size ranges (25–50 and 50–80 μm) of SiC particles have been used for synthesizing ADC-12–SiC composite. The volume fraction of SiC particles has been varied in the ranges from 5 to 15 wt%. It has been noted that the abrasive wear rate of the alloy reduced considerably due to addition of SiC particle and the wear rate of composite decreases linearly with increase in SiC content. It has also been noted that the wear resistance of composite varies inversely with square of the reinforcement size. The wear rate of the alloy and composite has been found to

be a linear function of applied load but invariant to the abrasive size; at critical abrasive size, transition in wear behaviour is noted.

Hassan et al. [16] investigated the effects of adding copper as alloying element and silicon carbide as reinforcement particles to Al–4 wt% Mg metal matrix. The friction and wear behavior of Al–Mg–Cu alloys and Al–Mg–Cu–based composites containing SiC particles were investigated at room conditions at a pressure of 3.18 MPa and a sliding speed of 0.393 m/s using a pin-on-disk wear testing machine. The wear loss of the copper containing alloys was less than that for the copper free alloys. It was observed that the volume losses in wear test of Al–Mg–Cu alloy decrease continuously up to 5%. Also it was found that the silicon carbide particles play a significant role in improving wear resistance of the Al–Mg–Cu alloying system. The formation of mechanically mixed layer (MML) due to the transfer of Fe from counterface disk to the pin was observed in both Al–Mg–Cu alloys and Al–Mg–Cu/SiC composites.

Okafor and Aigbodion [17] studied the properties of Al-4.5Cu/$ZrSiO_4$ particulate composite synthesized via squeezed casting route by varying the percentage $ZrSiO_4$ in the range of 5-25wt%. The result revealed that addition of $ZrSiO_4$ reinforcements increased the hardness value and apparent porosity by 107.65 and 34.23% respectively and decrease impact energy by 43.16 %. As the weight percent of $ZrSiO_4$ increases in the matrix alloy, the yield and ultimate tensile strength increased by 156.52 and 155.81% up to a maximum of 15% $ZrSiO_4$ addition respectively. The distribution of the brittle $ZrSiO_4$ phase in the ductile matrix alloy led to increase strength and hardness values. These results had shown that, additions of $ZrSiO_4$ particles to Al-4.5Cu matrix alloy improved properties.

Prabu et al. [18] investigated the effect of stirring speed and time on the microstrucutre and hardness of the composite. High silicon content aluminium alloy–silicon carbide metal matrix composite material, with 10%SiC were synthesized in the study, using different stirring speeds and stirring times. The microstructure of the produced composites was examined by optical microscope and scanning electron microscope. The Brinell hardness test was performed on the composite specimens from base of the cast to top. The results revealed that stirring speed and stirring time influenced the microstructure and the hardness of composite. Microstructure analysis revealed that at lower stirring speed with lower stirring time, the particle clustering was more. Increase in stirring speed and stirring time resulted in better distribution of particles. The hardness test results also revealed that stirring speed and stirring time have their effect on the hardness of the composite. The uniform hardness values were achieved at 600 rpm with 10 min stirring. But beyond certain stir speed the properties degraded again.

In the present work LM 13 alloy has been chosen for matrix alloy as it is used as commercial piston alloy and contains around 1% Mg which is necessary for wetting of dispersoid in the matrix. The reinforcement of silicon carbide (SiC) and zircon sand ($ZrSiO_4$) is used for the study of dual reinforced particle composite.

4. Matrix material

In the present study well known piston alloy LM13 is used as matrix material and high purity zircon sand ($ZrSiO_4$) and Silicon Carbide (SiC) as reinforcement. LM13 alloy was obtained in the form of ingots. The compositional analysis of the LM13 alloy was done by wet chemical analysis which is given in Table I.

Table I: Composition of the LM13 alloy in wt %

LM13 alloy	Si	Fe	Cu	Mn	Mg	Zn	Ti	Ni	Pb	Sn	Al
Wt %	11.8	0.3	1.2	0.4	0.9	0.2	0.02	0.9	0.02	0.005	Balance

4.1 Reinforcement material

Silicon carbide (SiC) and zircon sand ($ZrSiO_4$) particles were used as reinforcement material. Particle size of as received reinforcement was in the range between 50-200 µm. The reinforcement particle were ball milled to reduce the size and by sieving required particle size 20-32 µm were selected for the experimentation.

4.1.1 Zircon sand

Zircon sand consists of mostly zirconium silicate ($ZrSiO_4$) and some hafnium in addition to some rare earth elements, titanium minerals (Rutile, Ilmenite), monazite, etc. Zircon is used

chiefly for facing on foundry moulds to increase the resistance against metal penetration. Milled zircon is used in refractory paint for coating the outside of moulds. Zircon sand deposits have been found in abundance near Indian coastal regions of Kerala, Tamilnadu and Orissa. Zircon was found to be a promising candidate as reinforcement material for aluminium, zinc and lead based composites.

The following are main advantages of using Zircon Sand as reinforcement:

- High hardness,
- High modulus of elasticity,
- High temperature resistance (melting point of 2500oC),
- Acid corrosion resistance
- Excellent thermal stability.

The last property is important since fabrication processes require drastic changes in temperature and large volumetric changes due to phase transformations can cause debonding at the interface. Furthermore, zircon possesses a very low thermal expansion coefficient compared to most other ceramic oxides. Therefore, a change in temperature would not give rise to very high thermal stresses within zircon particles [25, 27]. The properties of zircon sand is given in Table III

Table II: Properties of zircon sand ($ZrSiO_4$) [25, 27]

Properties	Values
Melting Point (^{0}C)	2500
Limit of applications(^{0}C)	1850-1880
Hardness(Mohr's Scale)	7.5
Density(g/cm^3)	4.25
Linear coeff. of expansion(10^{-6} K)	4.5
Fracture toughness (MPa- m$^{1/2}$)	5
Crystal structure	Tetragonal

4.1.2 Silicon carbide

Silicon is the only chemical compound of carbon and silicon. It was originally produced by a high temperature electro-chemical reaction of sand and carbon. Silicon carbide is an excellent abrasive and has been produced and embedded into grinding wheels and other abrasive products for over one hundred years. Today the material has been developed into a high quality technical grade ceramic with very good mechanical properties. It is used in abrasives, refractory, ceramics and numerous high-performance applications. The material can also be made an electrical conductor and has applications in resistance heating, flame igniters and

electronic components. Silicon carbide is composed of tetrahedral of carbon and silicon atoms with strong bonds in the crystal lattice. This produces very hard and strong material. The high thermal conductivity coupled with low thermal expansion and high strength give this material exceptional thermal shock resistant qualities. Silicon carbide ceramics with little or no grain boundary impurities maintain their strength to very high temperatures, approaching 1600^0C with no strength loss [1-3, 13].

The following are main advantages of using Silicon carbide as reinforcement:

- Low density
- High strength
- Low thermal expansion
- High thermal conductivity
- High hardness
- High elastic modulus
- Excellent thermal shock resistance
- Superior chemical inertness

Some physical properties of silicon carbide are listed in Table III [13]

Table III: Properties of Silicon carbide (SiC)

Properties	Silicon carbide
Melting Point (^{0}C)	2200-2700
Limit of applications(^{0}C)	1400-1700
Hardness(Mohr's Scale)	9
Density(g/cm^3)	3.2
Linear coeff. of expansion(10^{-6} K)	4.5
Fracture toughness (MPa- m$^{1/2}$)	4.6
Crystal structure	hexagonal

4.2 Experimental Procedure

The composite was made by two step stir casting route. In this process the melt was allowed to solidify in the crucible itself and the mixture is again heated in a furnace to 50-60°C above liquids temperature. The melt is then mechanically stirred as in conventional stir casting. Required quantity of LM13 alloy was taken in a graphite crucible and melted in an electric furnace. The temperature of melt was raised to 750 °C. This molten metal was stirred using a

graphite impeller at a speed 630 rpm to create the vortex. The impeller blades were designed in such way that it creates vortex.

The ceramic particles used as reinforcement were taken in defined proportion and mixed properly by spatula. Particles prior to mixing were preheated at 450°C to drive off the moisture. After the formation of vortex in the melt, the particles were charged inside the vortex at the rate of 20–25 g/min. into the melt during stirring by impeller with the help of funnel kept on top of vortex. Zircon sand and silicon carbide particles of fine grade (20-30µm) were selected for present work. After mixing of particles the melt slurry is allowed to solidify in a graphite crucible at room temperature conditions. After solidification the mixture is again re-melted in a furnace to ensure that slurry is in fully liquid condition and then melt is stirred with impeller for 12-15 minutes. Similar type of synthesis of composite was earlier reported by various researchers [11, 32]. During production of composite, the amount of LM13 alloy, stirring duration and position of stirrer in the crucible were kept constant to minimize the contribution of variables related to stirring on distribution of second phase particles. The other detail of it is given in table IV.

Table IV: List of processing parameters

Melting temperature	750°C
Total Stirring time	22-25 minutes
Mixing time	8-10 minutes
Blade angle	45°
No. of blades	3
Position of stirrer	up to 2/3 depth in the melt

In our earlier work on spray forming it is observed that 15% reinforcement of zircon sand reinforced composite has given better property, so we have restricted the reinforcement up15% only [33]. Moreover, this is also in accordance with as reported earlier by Okafor and igbodion [30]. In order to compare and correlate the effect of dual particle reinforcement on mechanical and tribological properties, five different composites containing a total of 15wt% reinforcement in different proportion were fabricated and have been designated by alphabets. The reinforcement combinations are also given in Table V.

Table V: Reinforcement combination of composites

Composite	Total 15 wt% reinforcement	
	$ZrSiO_4$ (Wt% in total reinforcement)	SiC (Wt% in total reinforcement)
A	15	-
B	3.75	11.25
C	7.5	7.5
D	11.25	3.75
E	-	15

4.3 Material characterization

Dry sliding wear tests of the reinforced and unreinforced alloys were performed under the ambient temperatures between 30–35°C and relative humidity between 22–35%, using a pin-on-disc wear and friction monitor (Model TR-20, Ducom, Bangalore). The cylindrical shaped samples (30 x 9 mm) of composite were tested against the hardened EN32 steel disc having chemical composition (0.14% C, 0.52% Mn, 0.18% Si, 0.13% Ni, 0.05% Cr, 0.06% Mo, 0.019% P, 0.015% S, balance Fe) and hardness 65 HRC. Before testing, each specimen was ultrasonically cleaned in acetone.

The wear tests of specimen from each set of composite have been conducted up to 2,880 m of sliding distance at a constant sliding velocity of 1.6 m s^{-1} and under five different loads 1, 2, 3, 4 and 5 Kg. The microstructural analysis has been done with the help of both optical (Eclipse MA-100, Nikon) and scanning electron microscope at various magnifications (JEOL, JSM-6510LV, Japan). Electron dispersive spectroscopy (EDS) analysis of samples was also done at different phases. Before optical observation the sample was mechanically polished and etched by Keller's reagent for obtaining better contrast.

CHAPTER-5

RESULT & DISCUSSION

5.1 Microstructural Analysis

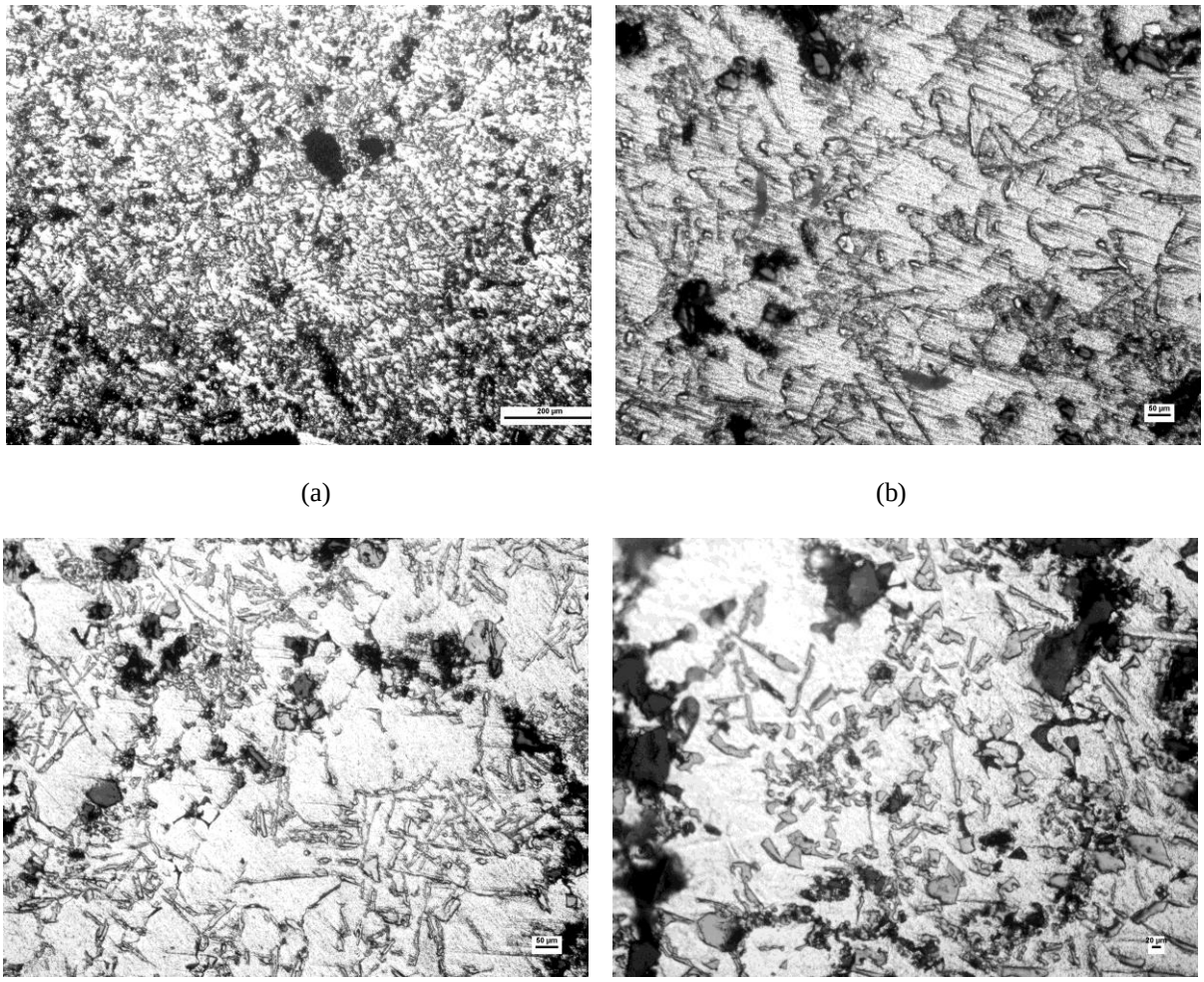

(a) (b)

(c) (d)

Fig.4: The Optical micrograph of composite 'A' containing 15% zircon sand. (a) Uniform particle distribution showing (b) networked like distribution of silicon (c) globular morphology of silicon in the vicinity of particle (d) less acicular and finely distributed silicon

The optical micrographs of composite 'A' reinforced with 15% zircon sand fine particles (20-32 μm) are shown in Fig.4. The Fig. 4(a) shows homogeneous distribution of reinforced particles in alloy matrix. Dendritic morphology is not observed and microstructure gets refined to cellular type morphology. Fine microstructural features are desired for achieving better wear behavior and mechanical properties.

Dendritic fragmentation can be attributed to the shearing of initial dendritic arms by the stirring action. During particle addition, local solidification of the melt occurs which is induced by the particles as there is a temperature difference between particle and the melt. It was also found that the perturbation in the solute field due to the presence of particles can change the dendrite tip radius and the dendrite tip temperature. These effects give rise to a dendrite to cell transition as the density of particles is increased. Also the length of the dendrite is reduced in the presence of the particles [7]. However, agglomeration of particles is also observed which is visible at certain places (Fig. 4 a, b).

Fig.4 (b) shows the micrograph of the composite where eutectic silicon distribution is observed, the eutectic silicon is having acicular morphology but it is less acicular or blunted type. Fig. 4(c) exhibits globular morphology of eutectic silicon having fine distribution as colonies around the reinforced particles. Particle clustering is also visible at some places, which is due to particle pushing by advancing solid-liquid interface [7, 34]. It is clear from Fig. 4(d) that eutectic silicon is having non-acicular morphology in the vicinity of the particle. The refinement of eutectic silicon can be attributed to the presence of magnesium in the base alloy and small amount of magnesium affect the solidification phenomena by increasing the cooling rate and hence promoting the refinement of eutectic silicon [35].

The optical micrographs of composite 'B' reinforced with 15% of SiC and Zircon sand particles are shown in Fig.5. The Fig.5 (a) shows the refined microstructure and homogeneous distribution of particles in the alloy matrix. Dendritic morphology is also absent in this composite microstructure. This can be attributed to the two step stir casting process in which prolonged time of mixing and stirring is bifurcated.

In the Fig.5 (b) colonies of eutectic silicon is seen in the vicinity of the particle. Moreover near the particle, eutectic silicon having globular morphology and blunted morphology is observed in the matrix. As compared to microstructure of only zircon sand reinforced composite, composite B exhibits better morphological features. As observed in Fig. 5(c) that each and every particle is having a colony of eutectic silicon which is indicative of the role of particles in nucleating the eutectic silicon. Zircon sand and SiC particles provide effective site for nucleation and also restricts the growth of dendrite and modifies the matrix with more refined structure leading to improvement in strength [36]. At higher magnification as shown in Fig. 5 (d) the globular and blunted morphology of eutectic silicon is observed. The distribution of eutectic silicon is also refined in the matrix alloy. Similar modification in silicon morphology was reported in earlier work by Kaur and Pandey [37] and attributed this morphological transformation to the localized rapid cooling effect produced by zircon sand particle due to large temperature difference in the melt around its vicinity.

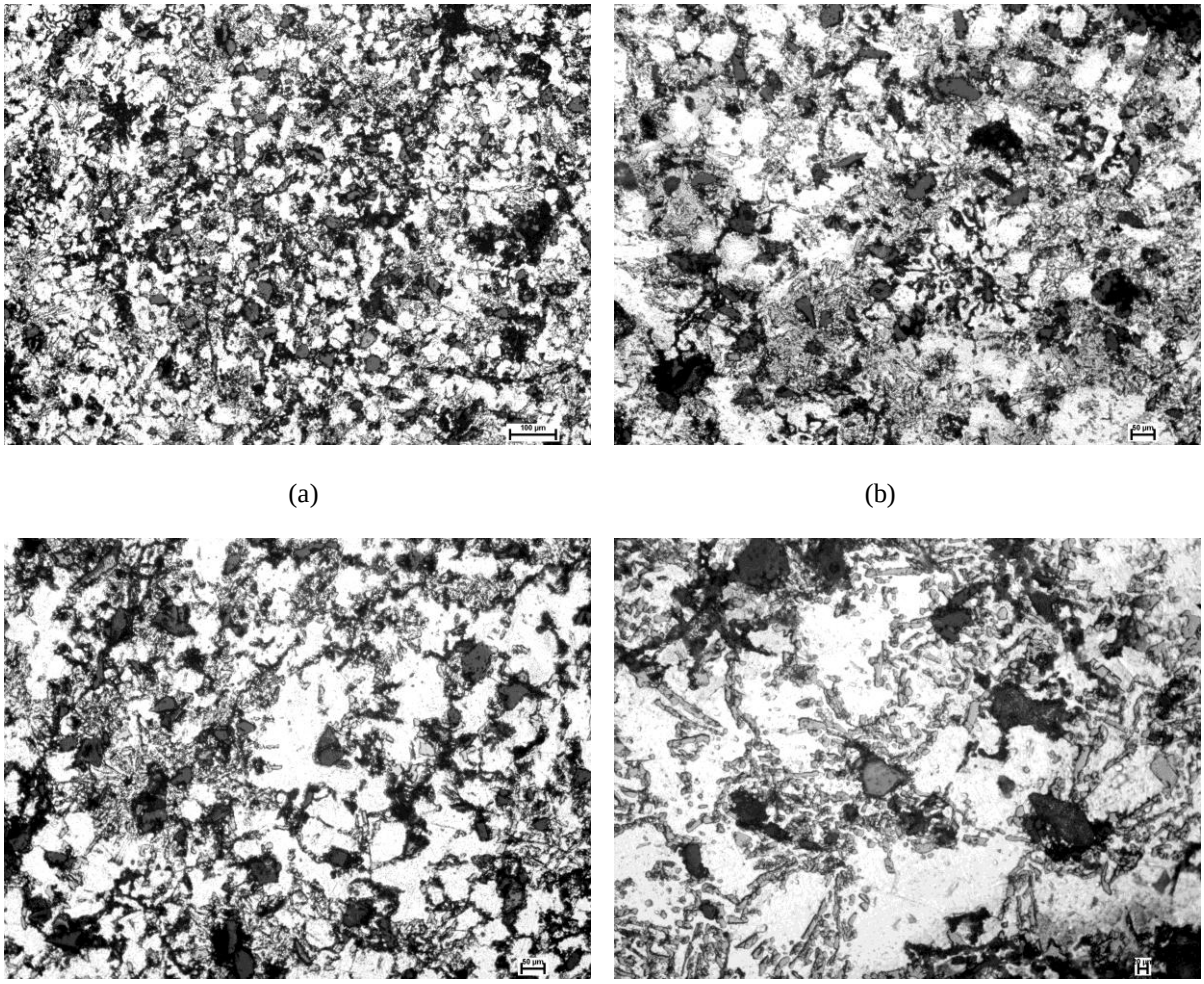

(a) (b)

(c) (d)

Fig.5: The Optical micrograph of composite 'B' containing 15% of silicon carbide and zircon sand particles showing (a) Uniform particle distribution of both the particles in the alloy matrix (b)segregation at finer scale of eutectic silicon around the particle (c) micro level clustering (d) both particle providing nucleation site for eutectic silicon

The optical micrographs of composite 'C' containing 15% of silicon carbide and zircon sand particles is shown in Fig. 6. It depicts the refinement of microstructure and eutectic silicon. Fig. 6(a) shows the homogeneous distribution of reinforced particles in the alloy matrix. Eutectic silicon along with dispersed particles is densely arranged in such a way that, they almost cover the entire matrix. The eutectic silicon becomes finer and nucleates near particles as colonies which can be seen in Fig. 6 (b & c).

Clustering of particles is observed at some places and the clustered particles have chip out during polishing the samples. However, fine particles have the tendency of clustering though it is not much pronounced in the prepared composites. In higher magnification micrograph as shown in Fig. 6(d) the eutectic silicon is finely distributed with blunted morphology.

Optical micrograph of composite 'D' containing 15% of SiC and zircon sand particles is shown in Fig.7. Finer distribution of eutectic silicon along with homogeneous distribution of particles can be seen (Fig.7 a). Eutectic silicon colonies around particle are more pronounced

in the micrograph as seen in Fig. 7 (b). In Fig. 7 (c) eutectic silicon distribution is more refined and morphology has changed from acicular to globular around the particles. Also in the matrix the eutectic silicon having blunted morphology as compared to long needle shape or acicular is seen. However, the fine particles and silicon form a network structure because of pushing interface from different nucleation sites as can be seen in Fig. 7 (d). Moreover, the clustering of fine particles at some places is also observed.

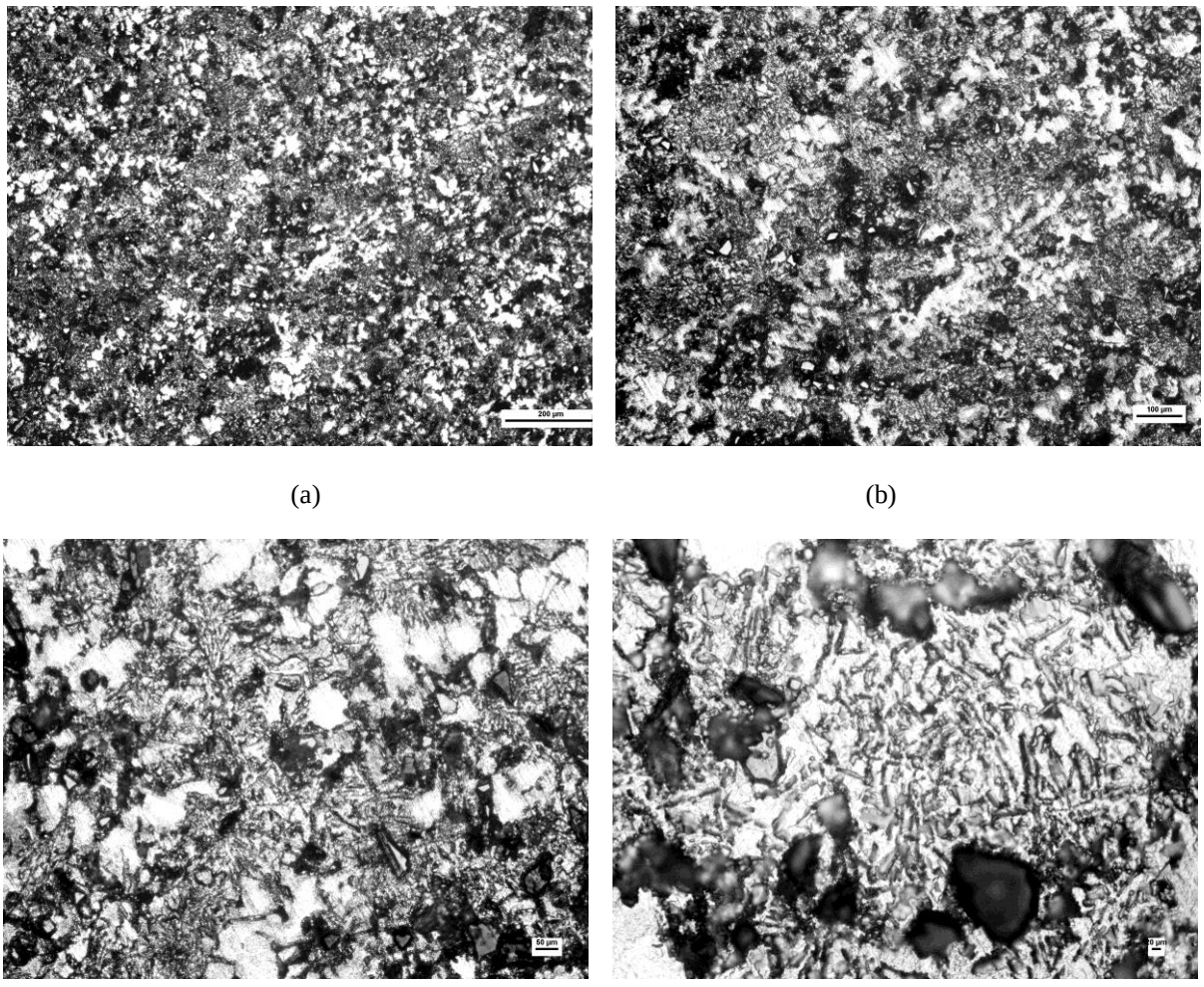

(a) (b)

(c) (d)

Fig.6: The Optical micrograph of composite 'C' containing 15% of SiC and Zircon sand particles showing (a) finely distribution of silicon throughout the matrix (b) silicon distributed at a very finer scale (c) globular silicon morphology around the particle (d) less acicular and finely distributed silicon in the vicinity of the particles.

Optical micrograph of composite ‘D’ containing 15% of SiC and zircon sand particles is shown in Fig.7. Finer distribution of eutectic silicon along with homogeneous distribution of particles can be seen (Fig.7 a). Eutectic silicon colonies around particle are more pronounced in the micrograph as seen in Fig. 7 (b). In Fig. 7 (c) eutectic silicon distribution is more refined and morphology has changed from acicular to globular around the particles. Also in the matrix the eutectic silicon having blunted morphology as compared to long needle shape or acicular is seen. However, the fine particles and silicon form a network structure because of pushing interface from different nucleation sites as can be seen in Fig. 7 (d). Moreover, the clustering of fine particles at some places is also observed.

Optical micrograph of composite ‘E’ containing 15% of SiC particles is shown in Fig.8. Fig. 8(a) shows that distribution of eutectic silicon is more refined and on finer scale as compared to other composite. Clustering is also observed at some places. In the Fig. 8(b) the eutectic silicon colonies network is observed. The majority of eutectic silicon is acquiring globular morphology and eutectic colonies are interconnected as observed in Fig. 8(c). At higher magnification it is clearly seen that eutectic silicon possessing globular morphological feature although few of them are having ellipsoidal or blunted morphology.

Overall analysis of structure indicates that microstructure is refined whereas eutectic silicon having blunted and globular morphological features. This refinement leads to better tribological and mechanical properties in the composite. The colonization of eutectic silicon in the vicinity of the particles enhances particle capability of wear resistance. The reinforced particles are uniformly distributed in the alloy matrix. The good bonding between particles and alloy matrix is also revealed in the micostructural analysis. Moreover porosity is at minimum level and not observed in the optical examination, although clustering is seen at same places in the composite. Microstructure analysis shows that addition of SiC has a pronounced effect on the microstructure and eutectic silicon refinement. The degree of microstructure and eutectic silicon refinement increases in accordance with the increase of SiC reinforced particle percentage. The most prominent feature observed in all composite is the absence of dendritic growth which is accounted for two step stircasting processing of the composites.

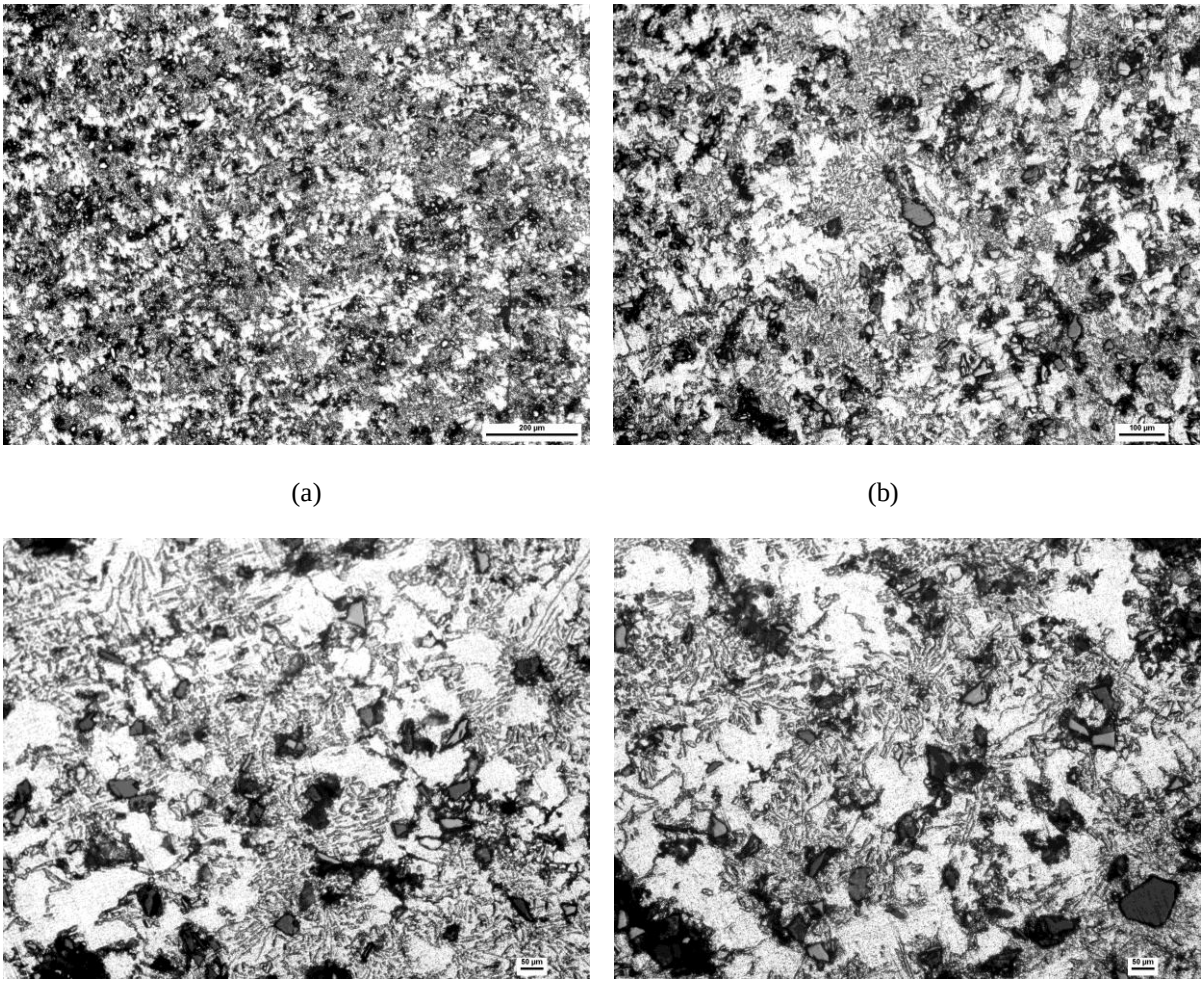

(a) (b)

(c) (d)

Fig.7: The Optical micrograph of composite 'D' containing 15% of SiC and Zircon sand particles showing (a) uniform distribution of both the particles (b) clustering at some places (c) globular and finer distribution of silicon around the particles (d) dense network of silicon exits around the particles.

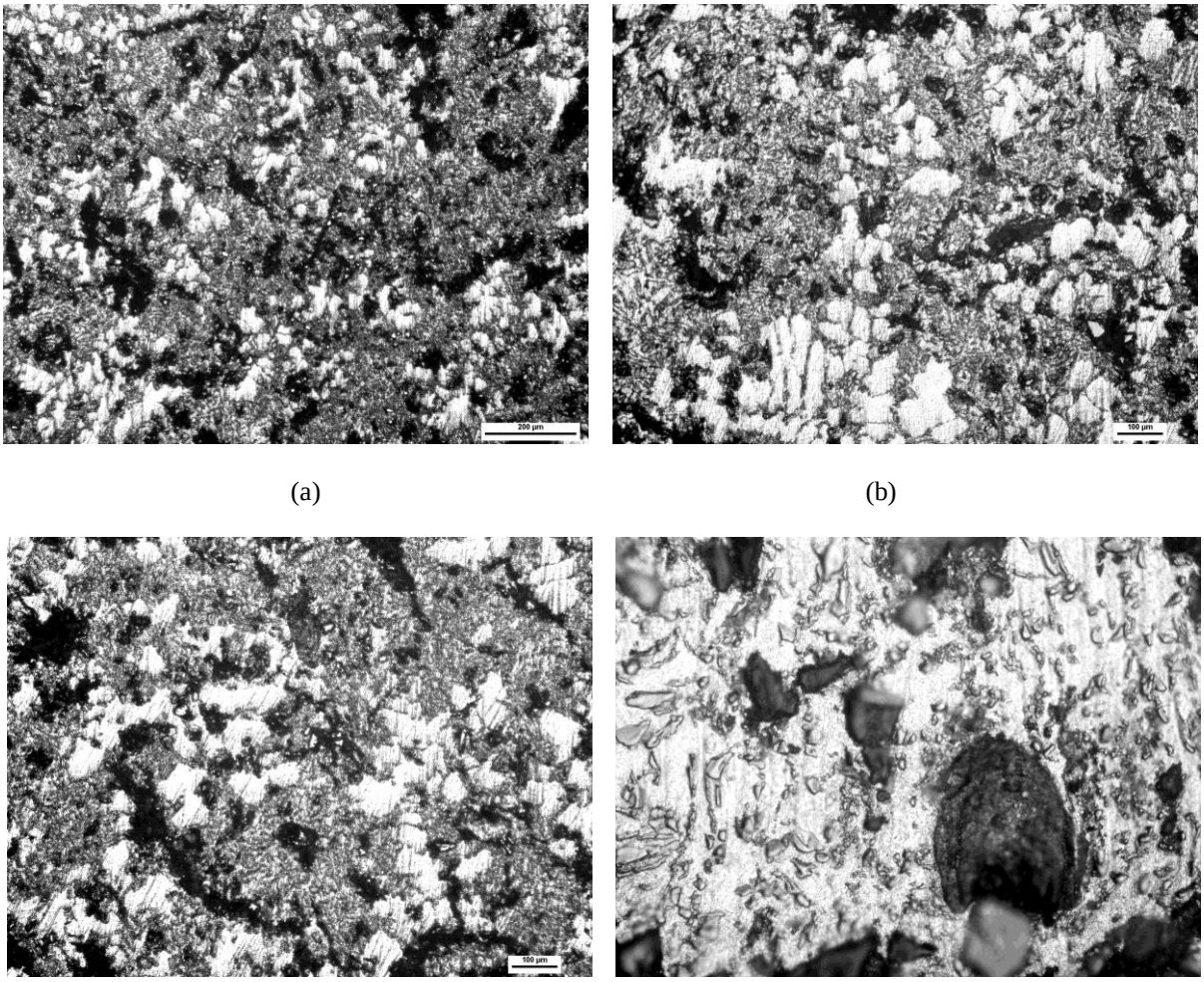

(a) (b)

(c) (d)

Fig.8: The Optical micrograph of composite 'E' containing 15% of SiC particles showing (a) finer distribution of eutectic silicon in the matrix (b) silicon at grain boundaries (c) clustering of particles (d) globular morphology of silicon around the particle.

5.2 Wear characteristics

5.2.1 Effect of sliding distance

The variation of wear rate with sliding distance of the composite has been studied at five different loads which are shown in Fig.9. It is observed that wear rate of the composites increases with the increase in applied load. The wear rate curve reveals two different type of wear behaviour under an applied load. The steep rise in the initial stage gives rise to greater wear corresponding to the run in wear. However, steady state wear is obtained in the later stage. Moreover, with increase in load the run-in and steady state wear rate are also found to increase.

The wear behavior of the composite A at different loads against sliding distance is shown in Fig. 9(a). It shows that at steady state wear is approachable after a sliding distance of 1000 meters. At 3 Kg load the wear rate increases and up to 2 Kg run-in wear increases uniformly afterwards it significantly increases at every increment in load. At 5Kg and1Kg load the wear rate is correspondingly decreases with sliding distance and approaches the steady state after 2500 meters of sliding distance. Steady state wear is approached after 1000 meters in case of 3 Kg and 4 Kg load.

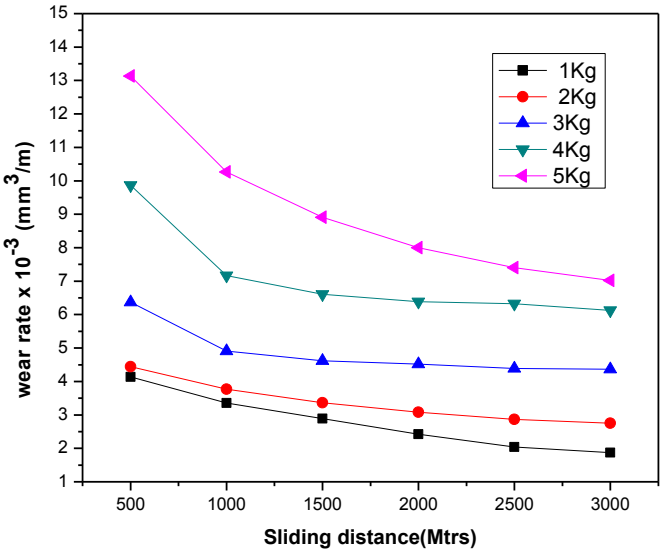

(a)

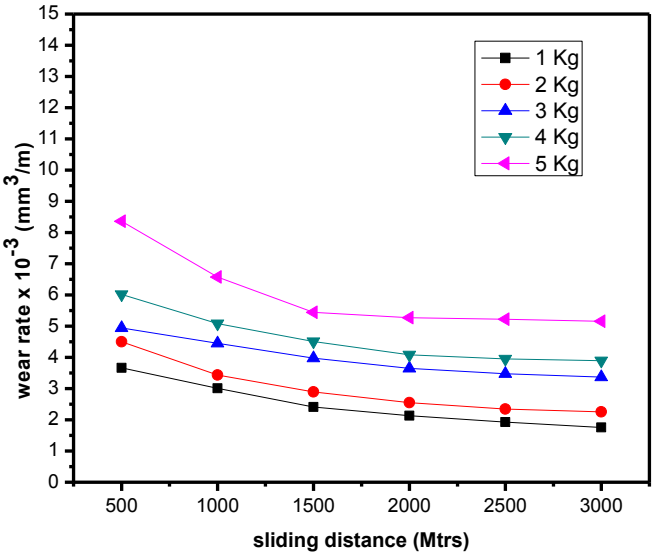
1 Kg
2 Kg
3 Kg
4 Kg
5 Kg
wear rate x 10^-3 (mm^3/m)
sliding distance (Mtrs)

(b)

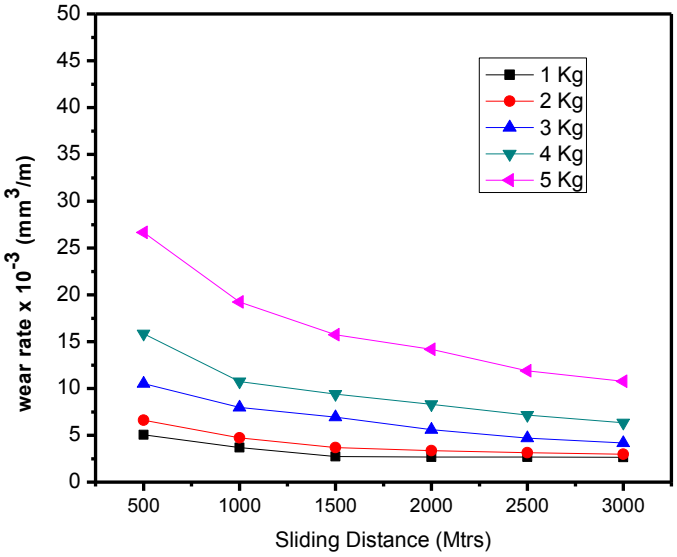
1 Kg
2 Kg
3 Kg
4 Kg
5 Kg
wear rate x 10^-3 (mm^3/m)
Sliding Distance (Mtrs)

(c)

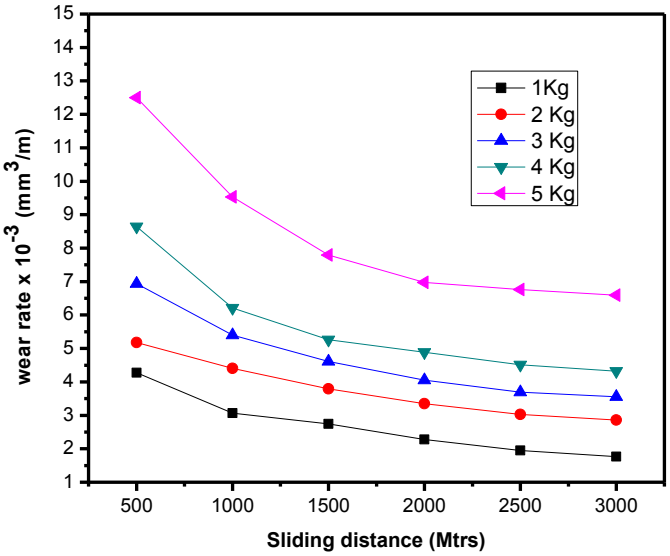

(d)

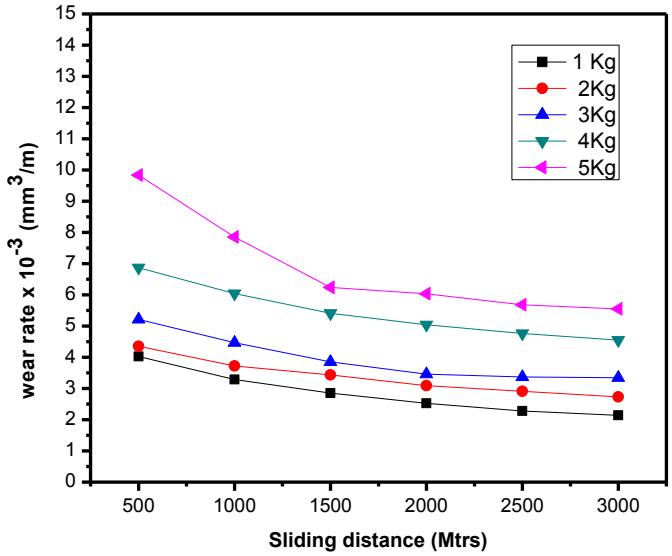

(e)

Fig.9: The graphical representation of wear rate of composite against sliding distance (a) composite A (b) composite B (c) composite C (d) composite D (e) composite E

Wear behavior of composite B which contains dual particle reinforcement is shown in Fig. 9(b). The run-in wear is low as compared to composite A at all loads. The steady state wear is approachable after the sliding distance of 1000 meters. The difference in wear rate of 1 Kg and 2 Kg, also in 3 Kg and 4 Kg is relatively small. The significant change of wear rate

occurs at 3 Kg load. At 5 Kg load steady state wear is reached at 1500 meters of sliding distance. As compared to composite A the composite B exhibits better wear behavior at all loads.

Wear rate of composite C against sliding distance is presented in Fig.9(c). The steady state wear is approachable after 1000 meters of sliding distance except at 5 Kg load, in which wear rate showing decreasing trend with respect to sliding distance. After 2 Kg load the wear rate show notable increase and continue up to 5 Kg load. The run-in wear in case of 4 Kg and 5 Kg load is high and at lower load it is relatively small. A high run-in wear is shown by this composite as compared to other composites under investigation. Wear behavior of composite D is different from the wear behavior of composite A, B and C as shown in Fig. 9(d). The run-in wear is high even at low loads whereas there is little run-in wear in previously discussed composites at low load. The steady state wear is observable after sliding distance of 2000 meters although wear rate is continuously decreasing with sliding distance up to 2000 meters. After every increment of load the wear rate increases uniformly except at 5 Kg which shows significantly high wear rate.

Wear characteristic of composite E is shown in Fig. 9(e). The run-in wear is very low at lower load. The steady state wear is approachable at sliding distance of 1000 meters except at 5 Kg load in which this stage is approached at sliding distance of 1500 meters. There is uniform increase in wear rate up to 3Kg load and afterwards it increases significantly. At lower load this composite shows better wear behavior as compared to composite D but it is not better as compared to composite A, B and C.

5.2.2 Comparison of wear behavior

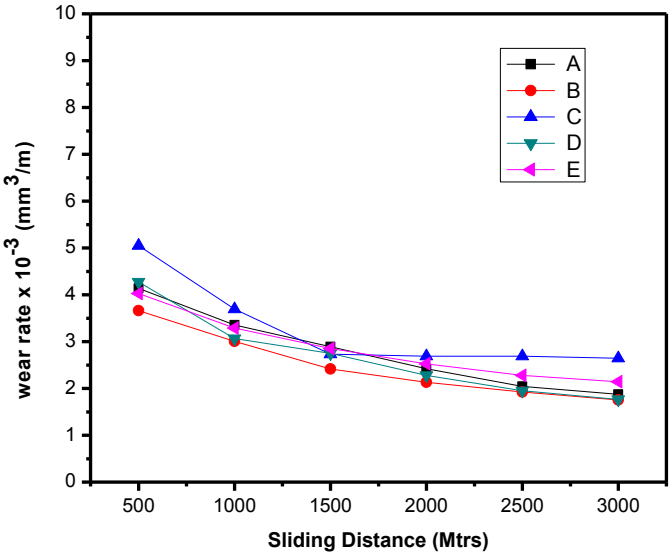

(a)

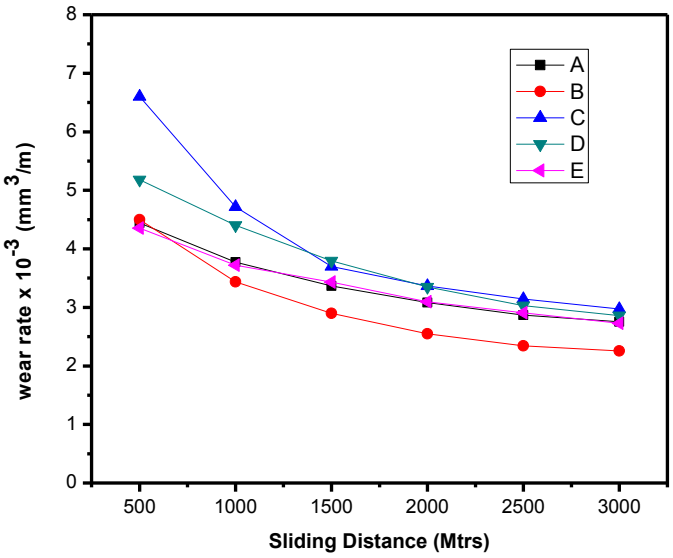

(b)

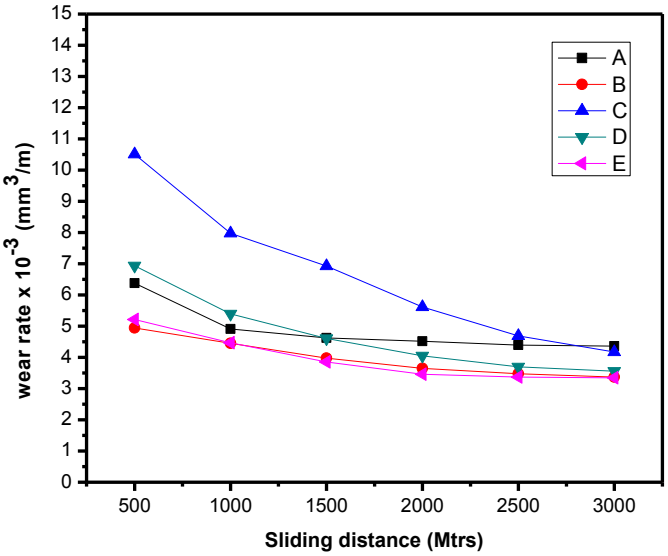
wear rate x 10^-3 (mm^3/m)
Sliding distance (Mtrs)
A
B
C
D
E

(c)

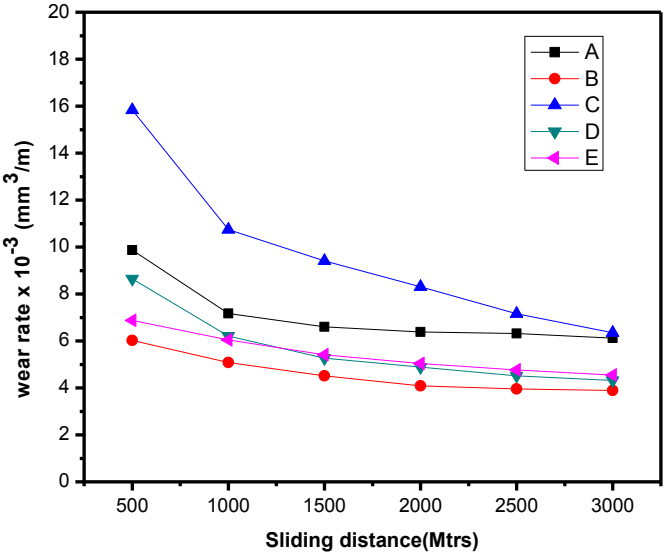
wear rate x 10^-3 (mm^3/m)
Sliding distance(Mtrs)
A
B
C
D
E

(d)

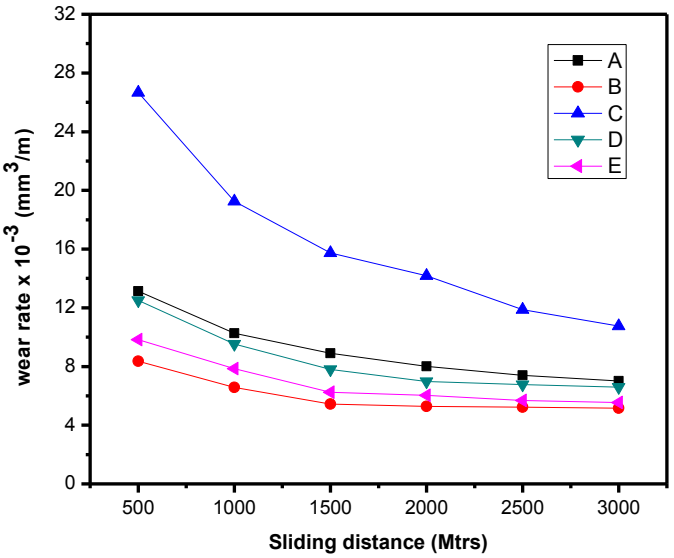

(e)

Fig.10: The comparison of wear rate of composites against sliding distance at various load (a)1Kg (b) 2Kg (c) 3Kg (d) 4Kg (e) 5Kg

The comparison of wear behavior of all the composites at different loads against sliding distance is shown in Fig. 10. Fig. 10(a) shows the comparison at 1 Kg load, it is observed that at this load composite B is exhibiting good wear resistance. However, the difference in wear rate is narrow. The run-in wear curve trend is almost similar due to same load but it is higher for composite C and lower for composite B. The composite A & E shows almost similar type of wear behavior as they contain single particle reinforcement. The steady state wear is approachable in almost all composite after sliding distance of 1500 meters.

The wear behavior of composite A & E are exactly same at 2Kg load as shown in Fig. 10(b). At 2Kg load the wear rate curve of composite A & E are coinciding even in run-in wear regime too, on the other hand composite B shows better wear resistance also at 2Kg load. Wear behavior of composite C & D is nearly similar but run-in wear is higher for composite C. The steady state wear is approachable after sliding distance of 1500 meters. Wear behavior of composites at 3Kg load is shown in Fig. 10(c). The wear behaviors of composite B and E are nearly same whereas the wear rate of composite C is very high. At this load composite B and E exhibits better wear resistance. Steady state wear is approached after sliding distance of 1000 meters. Composite A showing better steady state behavior and it shows better wear behavior as compared to wear behavior of composite C & D.

Wear behavior of composites at 4Kg load is shown in Fig. 10 (d). Fig. 10(d) shows that wear behavior of composite D and E are nearly same except in run-in wear regime. The composite

B shows better wear resistance and composite C shows high wear rate. The wear rate of composite A shows better steady state wear behavior but its wear resistance is good as compared to C only.

At 5Kg load the wear behavior of the composite is shown in Fig. 10 (e). All the composite exhibiting uniform wear behavior, the wear rate curve of all the composite are in same fashion except of composite C. The wear rate curve having narrow difference but wear rate becomes more than double as compared to low load wear rate. The composite B and E exhibits better wear resistance, composite A having better wear resistance as compared to composite C only while composite D showing better wear behavior at high load as compared to low load.

5.2.3 Nature of Wear Surface and debris

The morphologies of worn out surface of pins and debris offer clues to the wear mechanisms involved in sliding the sample against load. The Scanning electron microscope (SEM) micrographs of the composites tested at loads of 1, 3 & 5 kg at a speed of 1.6 m/s are presented in Fig. 11-15, which show the wear track morphology of the specimens tested.

One of the common feature observed in both lower and higher load, is the formation of grooves and ridges running parallel to the sliding direction in composites. On further analyzing it has been found that wear grooves are fine in worn pin surface of composite subjected to low load as compared to higher load. The depth of microploughing is increased on increasing load to 5 kg where contact asperities change the shape. Consequently the size and depth of the grooves become greater at this stage. However, at high loads the worn surfaces in some places shows patches from where the material was removed from the surface during the course of wear.

The Fig. 11 shows the SEM micrograph of worn pin of composite A at different loads. Fig. 11(a) shows that the worn surfaces are smooth and ploughing strips are very shallow on the surface. At this load higher magnification micrograph shows ploughing marks perpendicular to sliding direction as shown in Fig. 11(b). At 3 kg load, the craters are observed and ploughing marks got deeper as shown in Fig. 11(c). The material is removed from the alloy matrix by adhesive wear and delamination. Fig. 11(d) shows microcrack initiation and delamination of alloy matrix. At 5Kg load the ploughing marks become deeper and craters are observed as shown in Fig. 11(e). In Fig.11 (f) cracks are observed and excessive removal of material is seen. This behavior is characterized as severe wear behavior, in which material removal is accelerated.

SEM micrograph of worn pin of composite B at different loads is shown in Fig.12. Fig.12 (a) shows the ploughing marks with patches. At 1Kg load the ploughing marks are not deeper as compared to high load. The white small particles are also visible, which are originated from the rupture of mechanically mixed layer. Higher magnification micrograph at the same load is shown in Fig. 12 (b). Figure shows that microcrack are in the initial stage, there propagation

is not started at this load. However, small amount of material damage is observed by the delamination. At 3Kg load the craters grow in size as shown in Fig. 12(c). The ploughing marks become deeper and material removal is accelerated. Fig. 12(d) shows that several microcracks are propagating resulting in the removal of material by delamination. At 5Kg load the craters grow in the sliding direction with loss of material as shown in Fig. 12(e). Fig.12 (f) shows the white small flakes of mechanically mixed layer and removal of material by adhesive wear.

The Fig. 13 shows the SEM micrograph of worn pin of composite C at different loads. At 1Kg load composite C showing high wear as shown in Fig. 13(a). Long craters along the sliding direction are observed with white small particles of mechanically mixed layer. The material removal is shown by the craters in Fig. 13(b). At 3Kg load the small particles of mechanically mixed layer is shown in Fig. 13(c). Material removal is excessive as craters become deeper. Flakes of wear debris are also visible in this micrograph. At 5Kg load the material removal is excessive due to high load. The craters and ruptured mechanically mixed layer is observed in Fig. 13(d). The subsurface and surface cracks are visible in Fig. 13 (e). The crack propagation is along the sliding direction and also in perpendicular direction of sliding, which result in material removal by delamination. Higher magnification micrograph Fig. 13 (f) reveals the crater is growing in size by the crack formation.

The Fig. 14 shows the SEM micrograph of worn pin of composite D at different loads. At 1Kg load craters are formed along the sliding direction as shown in Fig. 14(a). Fig. 14(b) shows the material removal is by adhesive wear mechanism. At 3Kg load as shown in Fig. 14(c) the craters grow in size by successive material removal. In Fig. 14 (d) the corrugated type marks and long cracks are observed. At 5Kg load the excessive material is observed as shown in Fig. 14(e, f). Material loss by delamination occurs, small loosely held debris also seen in Fig.14 (e). Reinforced particles are also debonded and visible on the surface.

The Fig. 15 shows the SEM micrograph of worn pin of composite E at different loads. At 1Kg load ploughing marks with craters are shown in Fig. 15 (a). At 3Kg load surface damage by adhesive wear is observed in Fig. 15 (b). The ploughing marks are deeper but subsurface damage is not visible. Fig.15(c) shows that crack initiation is started along the edge of craters. At 5Kg load the ploughing marks are deeper and craters grow in size as shown in Fig. 15 (d-f).Ruptured mechanically mixed layer and debonded particles are seen in Fig. 15(e).

Composites wear debris SEM micrograph is shown in Fig.16. Wear debris of composite A at 4Kg load is shown in Fig. 16(a). Metallic flakes ranging from small to large in size and debonded zircon sand particles are seen. At 5Kg load the wear debris are corrugated type, this may be due to entrapment of debris during sliding as shown in Fig. 16(b). Wear debris of composite B is shown in Fig. 16(c-d). Long metallic flakes with debonded reinforced particles are seen in Fig. 16 (c). Some of debris which is having rugged edges as shown is generated by microcutting action. At 5Kg load the layered debris is seen in Fig. 16 (d). The layered debris is due to several microcracks caused by the sliding action. Some reinforced particles having spherical type shape due to entrapment of debris during sliding. Wear debris

of composite C is shown in Fig. 16(e-g). The metallic flakes along with debris generated by microcutting are observed in Fig. 16 (e). Matrix material is removed with embedded reinforced particles, material removed from the area of clustering. Microcutting chips with metallic flakes are seen in Fig. 16 (f). Fig.16 (g) shows the debris is of small size due to high load of 5Kg although large metallic and microcutting chips are also seen. Wear debris of composite D is shown in Fig.16 (h-i). At 4Kg long flakes with microcracks and microcutting flakes are seen in Fig. 16 (h). Material containing particles is also visible with debonded reinforced particles. In Fig. 16 (i) flakes generated by cutting action along with delaminated flakes are seen. The flakes having microcracks which show that the removal of material is due crack propagation. Wear of composite E is shown in Fig. 16 (j-l). Fig. 16 (j) shows fine debris with long flakes. Flakes generated by microcutting and crushed debris are seen in Fig.16 (k). Fig.16 (l) shows the long flakes with crushed flakes during sliding action. Some flakes are generated by microcutting action of hard particles.

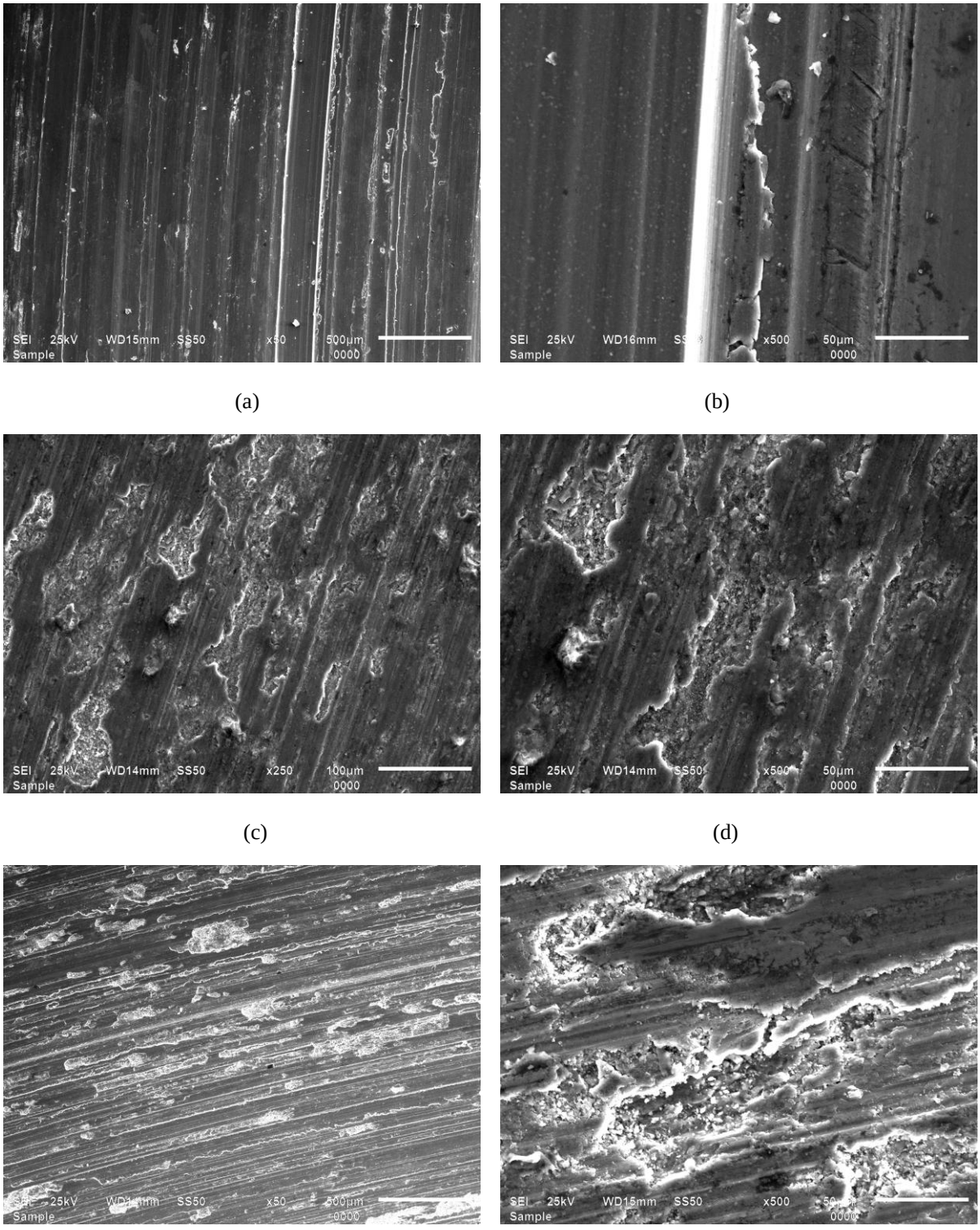

Fig.11: The SEM micrograph of worn pin surface of composite 'A' containing 15% of Zircon sand particles at (a) 1 Kg (b) 1 Kg (c) 3 Kg(d) 3 Kg (e) 5 Kg (f) 5 Kg

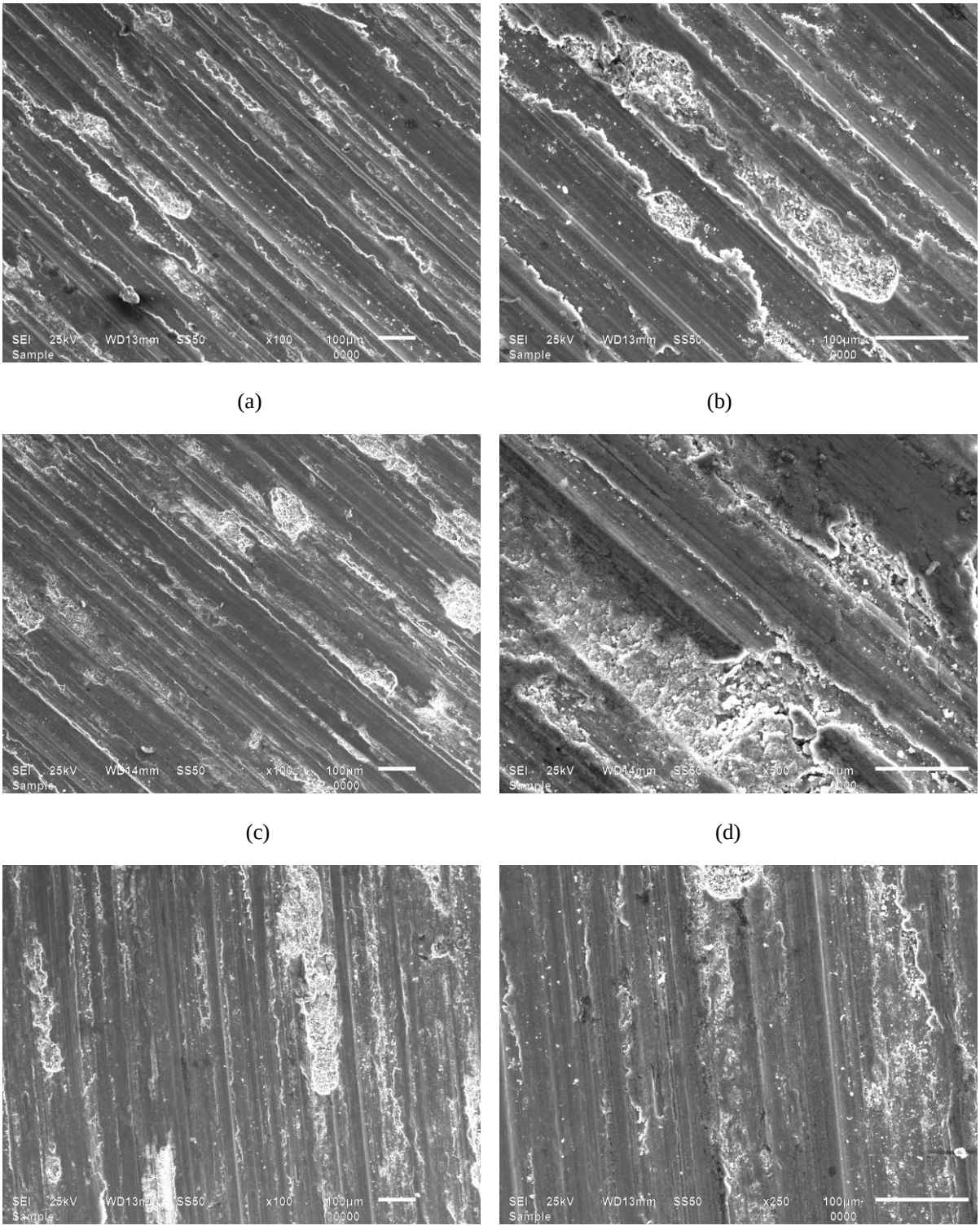

(a) (b)

(c) (d)

(e) (f)

Fig.12: The SEM micrograph of worn pin surface of composite 'B' containing 15% of Sic and zircon sand particles at (a) 1 Kg (b) 1 Kg (c) 3Kg (d) 3Kg (e) 5 Kg (f) 5 Kg

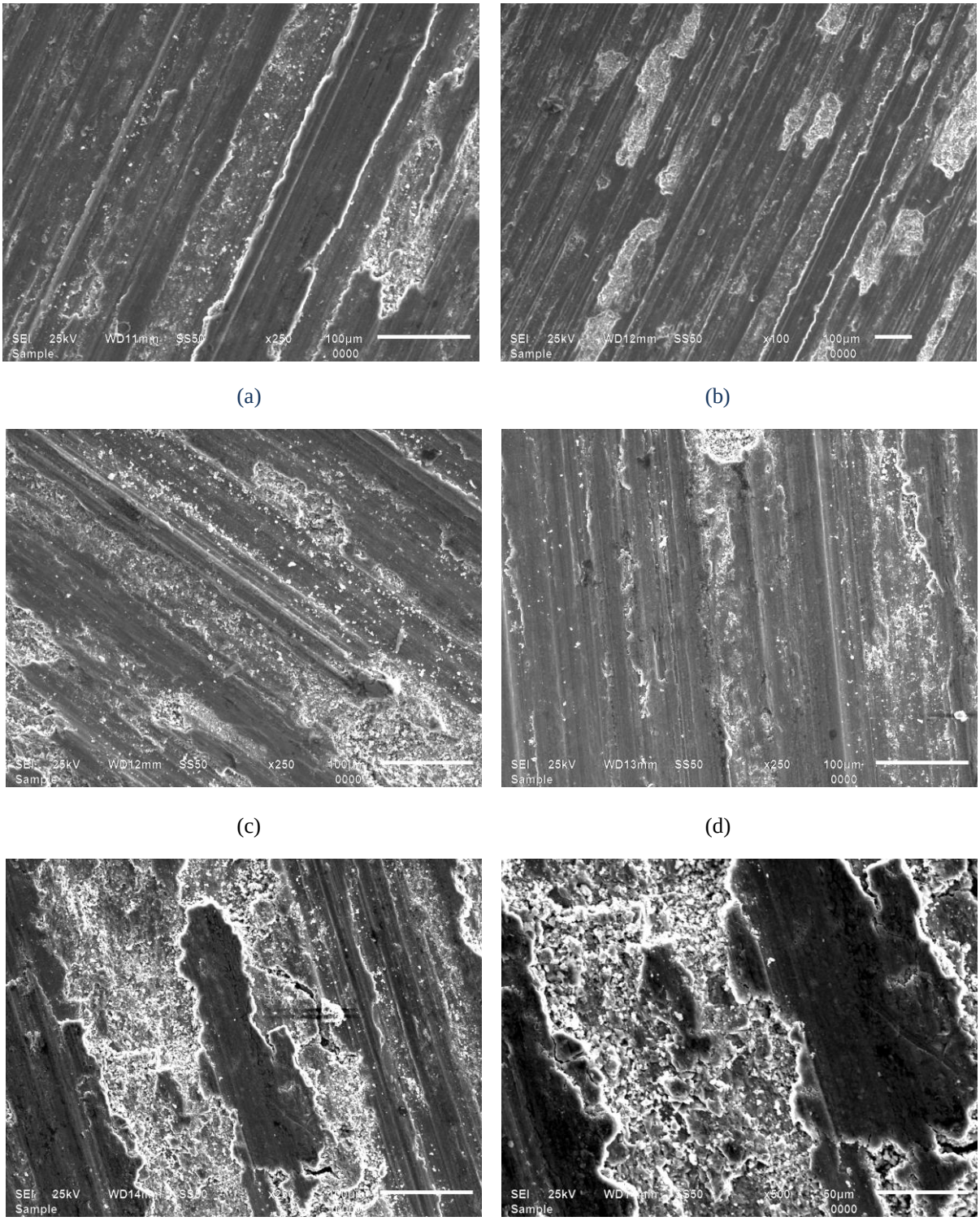

Fig.13: The SEM micrograph of worn pin surface of composite 'C' containing 15% of Sic and zircon sand particles at (a) 1Kg (b) 1Kg (c) 3 Kg (d) 5 Kg (e) 5 Kg (f) 5 Kg

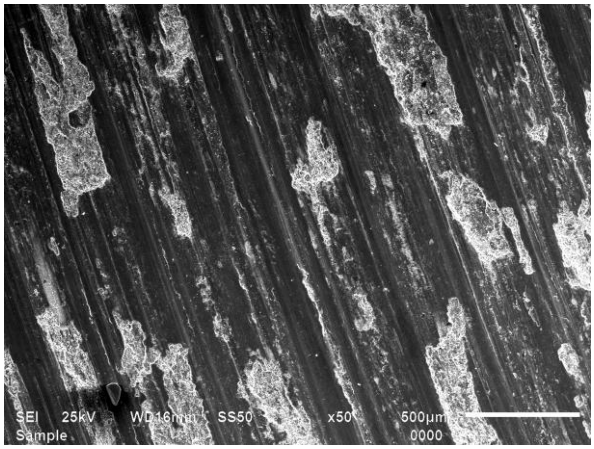

(a)

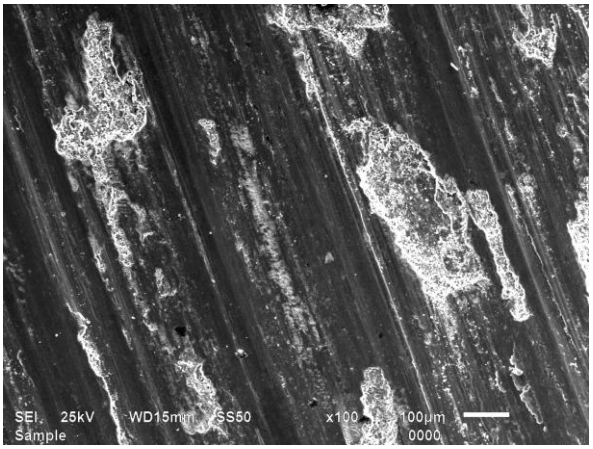

(b)

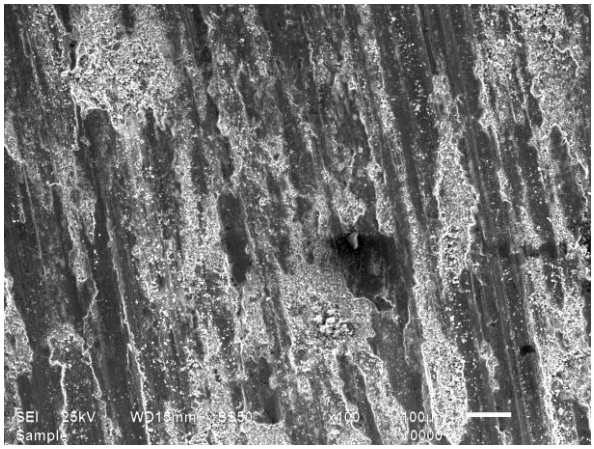

(c)

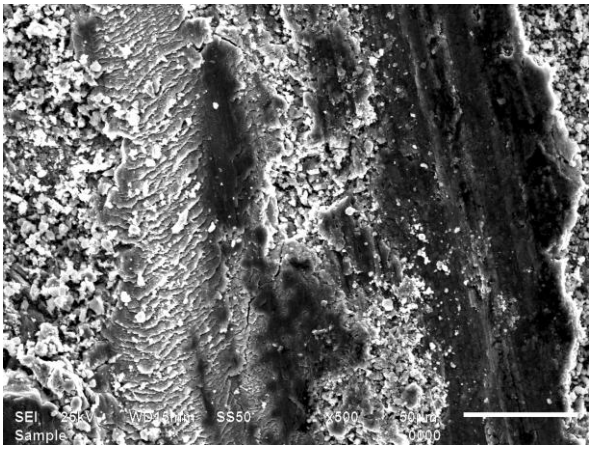

(d)

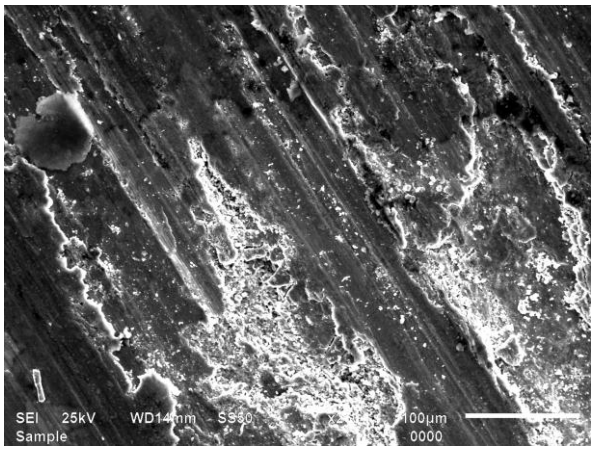

(e)

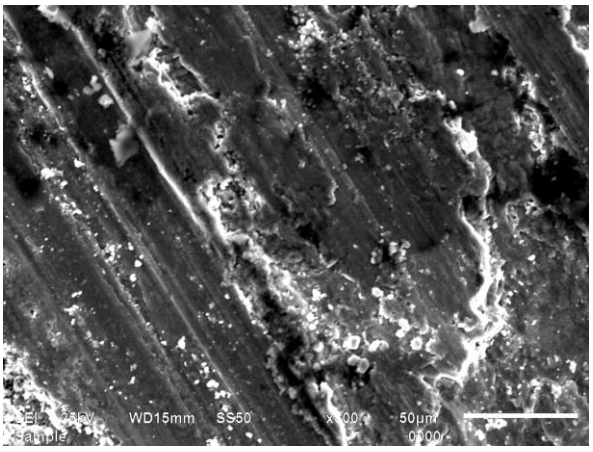

(f)

Fig.14: The SEM micrograph of worn pin surface of composite 'D' containing 15% of Sic and zircon sand particles at (a)1 Kg(b)1 Kg (c) 3 Kg (d) 3 Kg (e) 5 Kg (f) 5 Kg

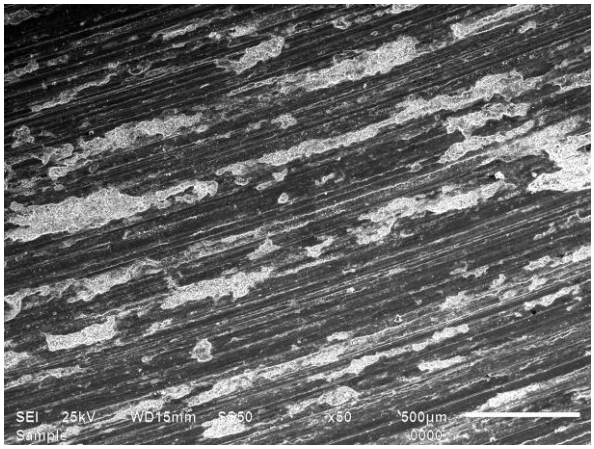

(a)

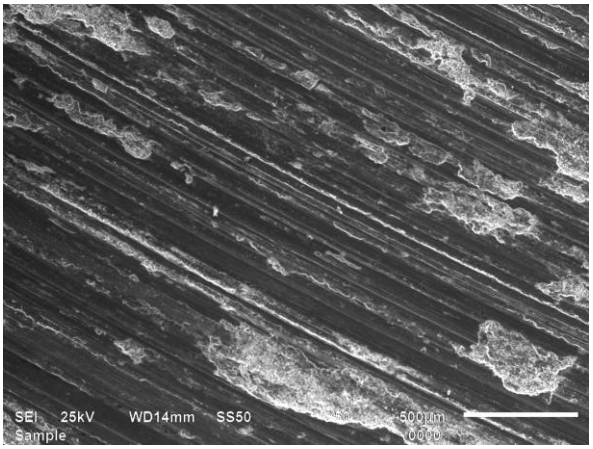

(b)

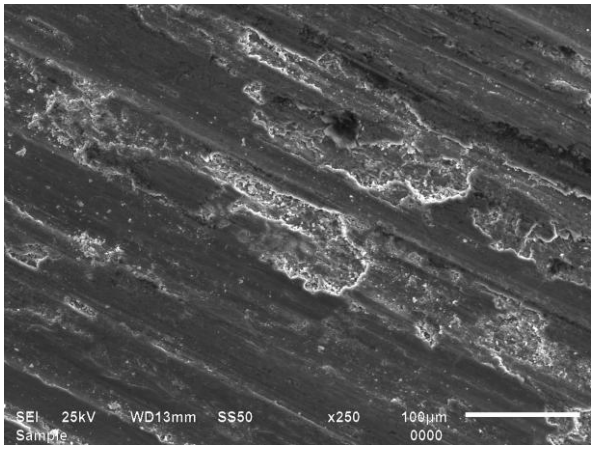

(c)

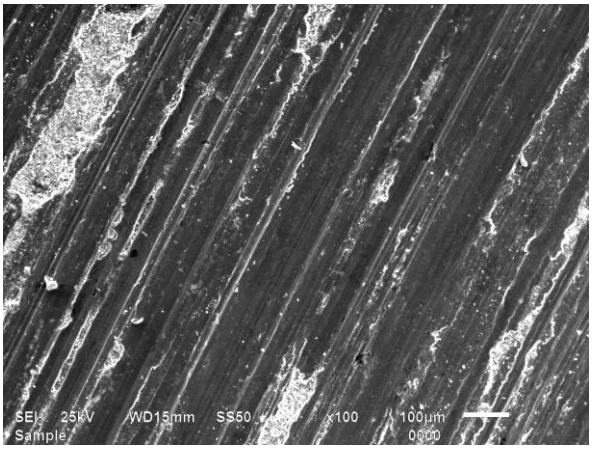

(d)

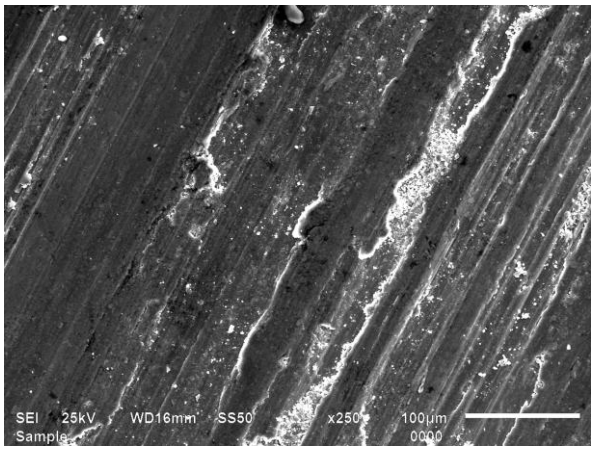

(e)

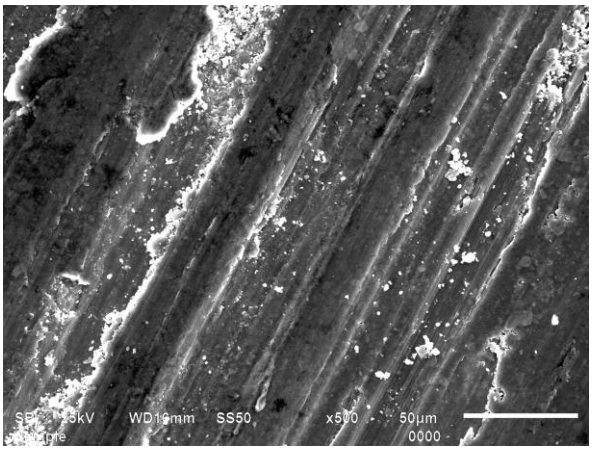

(f)

Fig.15: The SEM micrograph of worn pin surface of composite 'E' containing 15% of Sic particles at (a) 1 Kg (b) 3 Kg (c) 3 Kg (d) 5 Kg (e) 5 Kg (f) 5 Kg

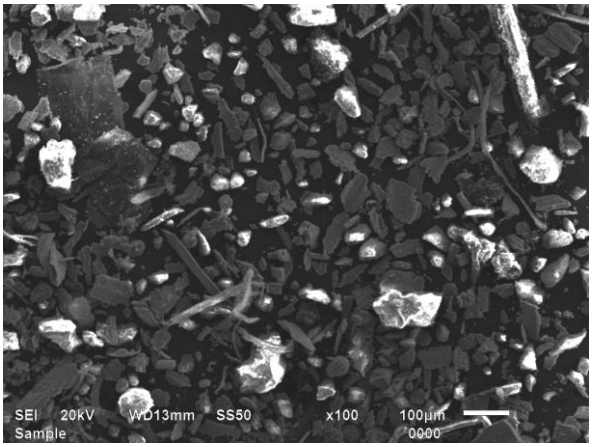
SEI 20kV WD13mm SS50 x100 100µm
Sample 0000

(a)

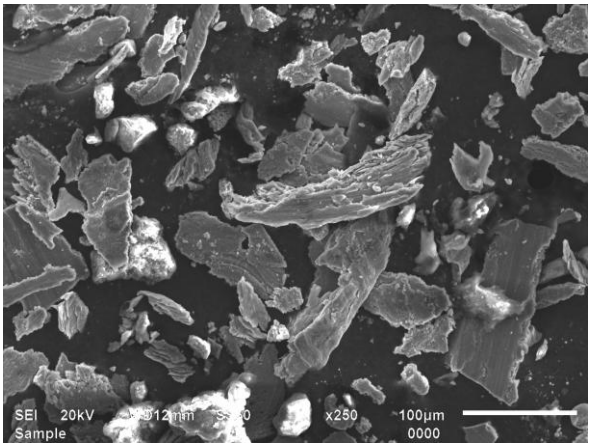
SEI 20kV WD12mm SS50 x250 100µm
Sample 0000

(b)

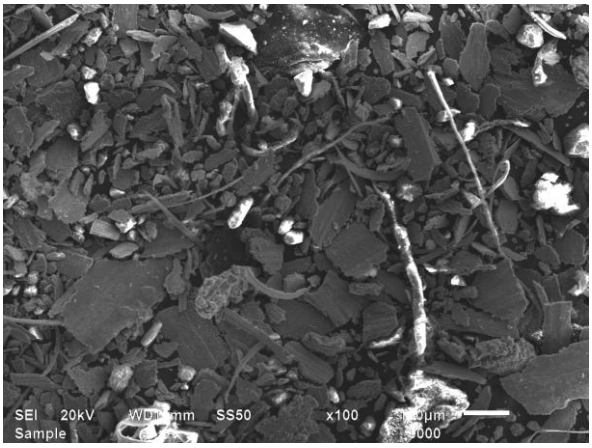
SEI 20kV WD13mm SS50 x100 100µm
Sample 0000

(c)

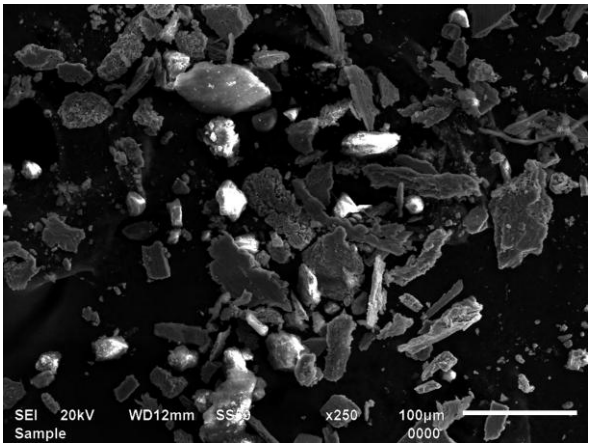
SEI 20kV WD12mm SS50 x250 100µm
Sample 0000

(d)

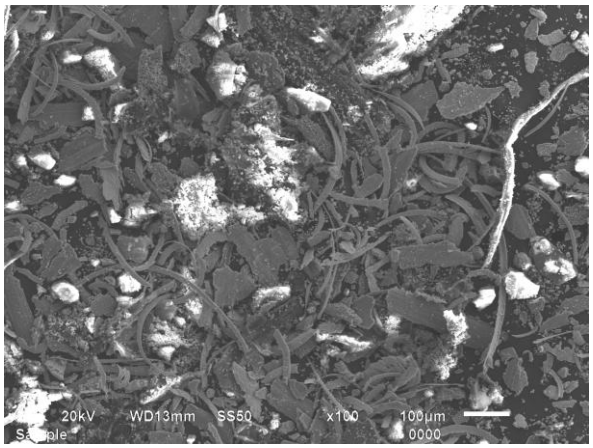
20kV WD13mm SS50 x100 100µm
0000

(e)

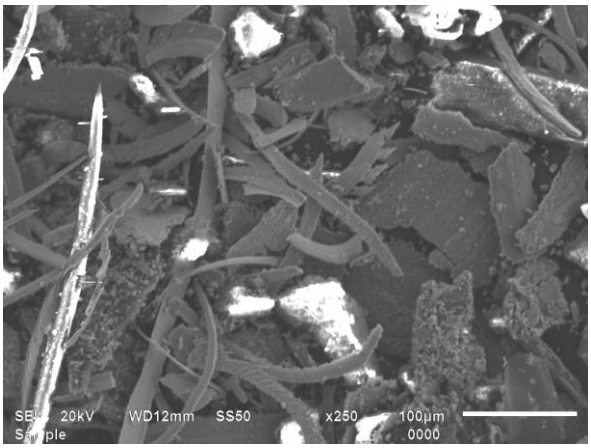
20kV WD12mm SS50 x250 100µm
0000

(f)

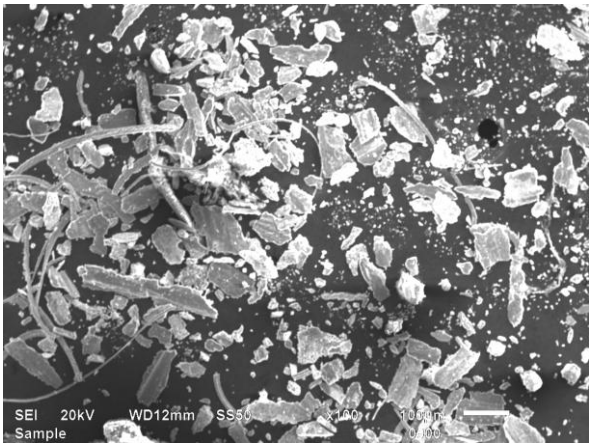

(g)

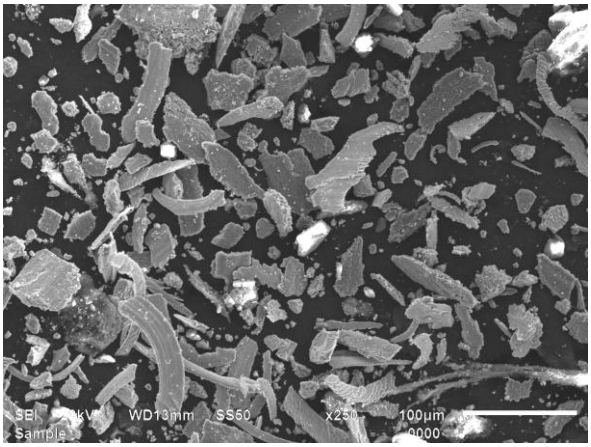

(h)

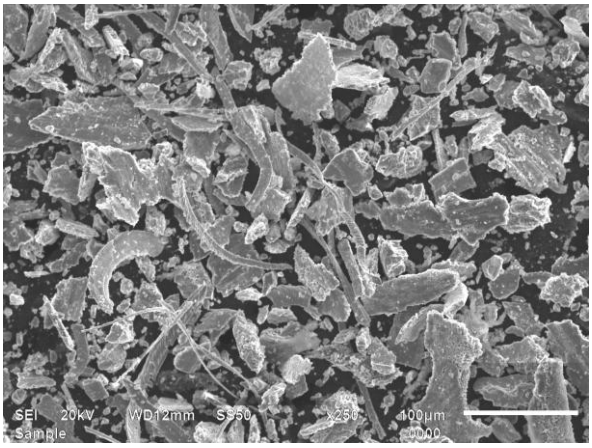

(i)

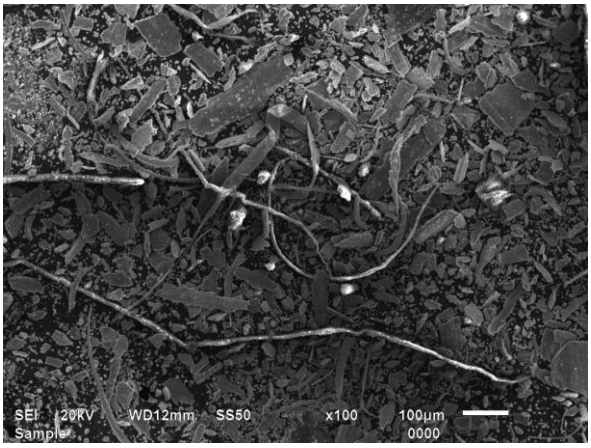

(j)

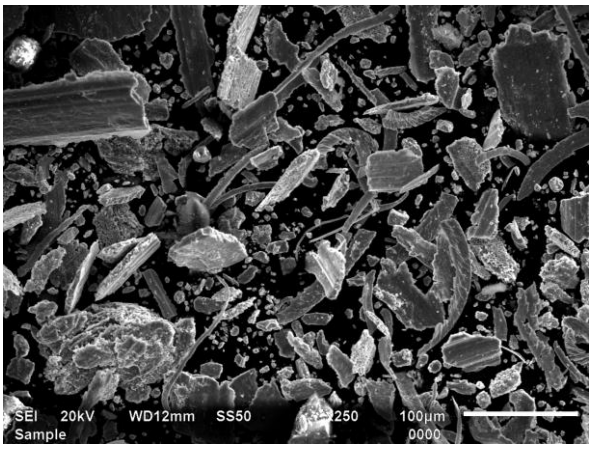

(k)

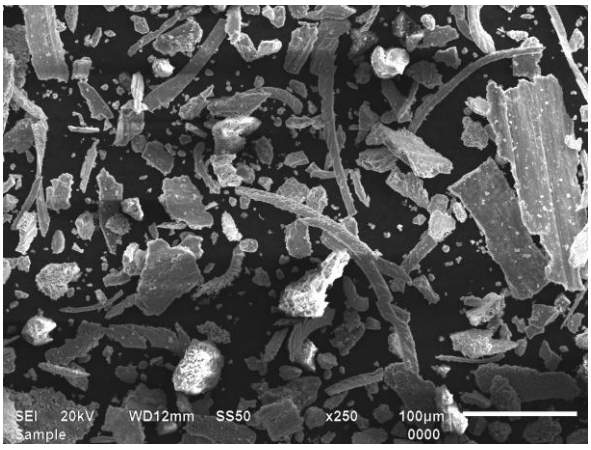

(l)

Fig.16: The SEM micrograph of wear debris (a) composite A at 4Kg (b) composite A at 5Kg (c) composite B at 4Kg (d) composite B at 5Kg (e) composite C at 3Kg (f) composite C at 3Kg (g) composite C at 5Kg (h) composite D at 4Kg (i) composite D at 5Kg (j) composite E at 2Kg (k) composite E at 3Kg (l) composite E at 5Kg

REFRENCES

[1] Composites, ASM Handbook, Volume 21

[2] F. C. Campbell, Manufacturing Processes for Advanced Composites, 2004 Elsevier Ltd.

[3] Guneri Akovali, Handbook of Composite Fabrication, 2001Rapra Technolgy Ltd.

[4] Mohamed A. Taha, Industrialization Of Cast Aluminum Matrix Composites (AMCCs), Materials and Manufacturing Processes, (2001)16: 5, 619 — 641

[5] M K SURAPPA, Aluminium matrix composites: Challenges and Opportunities, *Sadhana* Vol. 28, Parts 1 & 2, February/April 2003, pp. 319–334.

[6] J. Hashim, L. Looney, M.S.J. Hashmi, Metal matrix composites: production by the stir casting method, Journal of Materials Processing Technology 92-93 (1999) 1-7

[7] J. Hashim, L. Looney, M.S.J. Hashmi, Particle distribution in cast metal matrix composites—Part I, Journal of Materials Processing Technology 123 (2002) 251–257

[8] Md. Aminul Islam, Zoheir N. Farhat, Effect of porosity on dry sliding wear of Al–Si alloys, Tribology International 44 (2011) 498–504

[9] S. N. Aqida, M. I. Ghazali, J. Hashim, Effects Of Porosity On Mechanical Properties Of Metal Matrix Composite: An Overview, *Jurnal Teknologi*, 40(A) Jun. 2004: 17–32

[10] J. Hashim, L. Looney, M.S.J. Hashmi, The wettability of SiC particles by molten aluminium alloy, Journal of Materials Processing Technology 119 (2001) 324-328

[11] Jasmi Hashim, The Production of Cast Metal Matrix Composite by A Modified Stir Casting Method, *Jurnal Teknologi*, 35(A) Dis. 2001: 9–20

[12] Yan Wang, Hui-Yuan Wang, Kun Xiu, Hong-Ying Wang, Qi-Chuan Jiang, Fabrication of TiB2 particulate reinforced magnesium matrix composites by two-step processing method, Materials Letters 60 (2006) 1533-1537

[13] W. Zhou, Z.M. Xu, Casting of SiC Reinforced Metal Matrix Composites, Journal of Materials Processing Technology 63 (1997) 358-363

[14] R.N. Rao, S. Das, Effect of sliding distance on the wear and friction behavior of as cast and heat-treated Al–SiCp composites, Materials and Design 32 (2011) 3051–3058

[15] Dong Lu, J.P. Celis, S. Kenzari, V. Fournée, D.B. Zhou, Tribological behavior of aluminum matrix composites containing complex metallic alloys AlCuFeB or AlCuFeCr particles, Wear 270 (2011) 528–534

[16] M. Sameezadeh, M. Emamy and H. Farhangi, Effects of particulate reinforcement and heat treatment on the hardness and wear properties of AA 2024-$MoSi_2$ nanocomposites, Materials & Design Volume 32, Issue 4, April 2011, Pages 2157-2164

[17] S. Suresha , B.K. Sridhara,Wear characteristics of hybrid aluminium matrix composites reinforced with graphite and silicon carbide particulates, Composites Science and Technology 70 (2010) 1652–1659

[18] Aleksandar Vencla, Ilija Bobicb, Saioa Arostegui, Biljana Bobic, Aleksandar Marinkovi, Miroslav Babi, Structural, mechanical and tribological properties of A356 aluminium alloy reinforced with Al2O3, SiC and SiC + graphite particles, Journal of Alloys and Compounds 506 (2010) 631–639

[19] A. Urena, J. Rams, M. Campo, M. Sanchez, Effect of reinforcement coatings on the dry sliding wear behavior of aluminium/SiC particles/carbon fibres hybrid composites, Wear 266 (2009) 1128–1136

[20] Elliot Law, Sze Dai Pang, Ser Tong Quek, Discrete dislocation analysis of the mechanical response of silicon carbide reinforced aluminum nanocomposites, Composites: Part B 42 (2011) 92–98

[21] V.R. Rajeev, D.K.Dwivedi, S.C.Jain Dry reciprocating wear of Al–Si–SiCp composites: A statistical analysis, Tribology International 43 (2010) 1532–1541

[22] T.P.D. Rajan, R.M. Pillai, B.C. Pai, Characterization of centrifugal cast functionally graded aluminum-silicon carbide metal matrix composites, Materials Characterization 61(2010)923-928

[23] Md. Aminul Islam, ZoheirN.Farhat, Effect of porosity on dry sliding wear of Al–Si alloys, Tribology International 44(2011) 498-504

[24] Hirotaka Kato, Severe–mild wear transition by supply of oxide particles on sliding surface, Wear 255 (2003) 426-429

[25] Sanjeev Das, Siddhartha Das, Karabi Das, Abrasive wear of zircon sand and alumina reinforced Al-4.5 wt% Cu alloy matrix composites-A comparative study, Composites Science and Technology 67 (2007) 746–751

[26] S.C. Sharma, B.M. Girish, D.R. Somashekar, B.M. Satish, Rathnakar Kamath, Sliding wear behaviour of zircon particles reinforced ZA-27 alloy composite materials, Wear 224 (1999) 89–94

[27] Ashutosh Sharma, Sanjeev Das, Study of age hardening behavior of Al–4.5 wt%Cu/zircon sand composite in different quenching media – A comparative study, Materials and Design 30 (2009) 3900–3903

[28] D.P. Mondal, S. Das, High stress abrasive wear behaviour of aluminium hard particle composites: Effect of experimental parameters, particle size and volume fraction, Tribology International 39 (2006) 470-478

[29] Adel Mahamood Hassan, Abdalla Alrashdan, Mohammed T. Hayajneh, Ahmad Turki Mayyas, Wear behavior of Al–Mg–Cu–based composites containing SiC particles, Tribology International 42 (2009) 1230–1238

[30] E. G. Okafor , V. S. Aigbodion, Effect of Zircon Silicate Reinforcements on the Microstructure and Properties of as Cast Al-4.5Cu Matrix Particulate Composites Synthesized via Squeeze Cast Route, Tribology in industry, Volume 32, No. 2, 2010

[31] S. Balasivanandha Prabu , L. Karunamoorthy , S. Kathiresan , B. Mohan,Influence of stirring speed and stirring time on distribution of particles in cast metal matrix composite, Journal of Materials Processing Technology 171 (2006) 268–273

[32] W. Zhou, Z. M. Xu, Casting of SiC Reinforced Metal Matrix Composites, Journal of Materials Processing Technology 63 (1997) 358-363

[33] Kamalpreet Kaur, O. P. Pandey, Dry Sliding Wear Behavior of Zircon Sand Reinforced Al–Si Alloy, Tribol. Lett. (2010) 38:377–387

[34] Y.M. Youssef, R.J. Dashwood, P. D. Lee, Effect of clustering on particle pushing and solidification behavior in TiB2 reinforced aluminium PMMCs, Composites: Part A 36 (2005) 747–763

[35] T.P.D. Rajan, K. Narayan Prabhu, R.M. Pillai, B.C. Pai, Solidification and casting/mould interfacial heat transfer characteristics of aluminum matrix composites, Composites Science and Technology 67 (2007) 70–78

[36] J. Hashim, L. Looney, M.S.J. Hashmi: Particle distribution in cast metal matrix composites-Part II. Journal of Materials Processing Technology 12 (2002) 258–263

[37] K. Kaur, O. P. Pandey: Wear and microstructural characteristics of spray atomized zircon sand reinforced LM13 alloy. Mat.-wiss. u.Werkstofftech. 2010, 41, No. 7